



Article

*These authors contributed equally to this work.

Cite this article: Blard P-H et al. (2023). Basal debris of the NEEM ice core, Greenland: a window into sub-ice-sheet geology, basal ice processes and ice-sheet oscillations. *Journal of Glaciology* 69(276), 1011–1029. <https://doi.org/10.1017/jog.2022.122>

Received: 2 July 2022

Revised: 16 November 2022

Accepted: 19 December 2022

First published online: 17 May 2023

Keywords:




Basal ice; glacial sedimentology; ice core

Corresponding authors:

Pierre-Henri Blard; Email: blard@crpg.cnrs-nancy.fr;

Marie Protin; Email: marie.protin@univ-lorraine.fr

Basal debris of the NEEM ice core, Greenland: a window into sub-ice-sheet geology, basal ice processes and ice-sheet oscillations

Pierre-Henri Blard^{1,2,*} , Marie Protin^{1,*}, Jean-Louis Tison², François Fripiat², Dorthe Dahl-Jensen³, Jørgen P. Steffensen³ , William C. Mahaney⁴, Paul R. Bierman⁵, Andrew J. Christ^{5,6} , Lee B. Corbett⁵, Vinciane Debaille⁷, Thomas Rigaudier¹, Philippe Claeys⁸ and ASTER Team⁹

¹CRPG, Université de Lorraine, CNRS, F-54000 Nancy, France; ²Laboratoire de Glaciologie, Université Libre de Bruxelles, 1050 Brussels, Belgium; ³Centre for Ice and Climate, Niels Bohr Institute, University of Copenhagen, Juliane Maries Vej 30, 2100 Copenhagen K, Denmark; ⁴Quaternary Surveys, 26 Thornhill Ave., Thornhill, ON L4J1J4, Canada; ⁵Rubenstein School for the Environment and Natural Resources, University of Vermont, Burlington, VT, USA; ⁶Gund Institute for Environment, University of Vermont, Burlington, VT, USA; ⁷Laboratoire G-Time, Université Libre de Bruxelles, Brussels, Belgium; ⁸Analytical-Environmental & Geo-Chemistry, Vrije Universiteit Brussel, Brussels, Belgium and ⁹CEREGE, Aix Marseille Université, CNRS, IRD, INRAE, Coll France, 13545 Aix-en-Provence, France

Abstract

We present new data from the debris-rich basal ice layers of the NEEM ice core (NW Greenland). Using mineralogical observations, SEM imagery, geochemical data from silicates (meteoric ¹⁰Be, ϵ Nd, ⁸⁷Sr/⁸⁶Sr) and organic material (C/N, δ^{13} C), we characterize the source material, succession of previous glaciations and deglaciations and the paleoecological conditions during ice-free episodes. Meteoric ¹⁰Be data and grain features indicate that the ice sheet interacted with paleosols and eroded fresh bedrock, leading to mixing in these debris-rich ice layers. Our analysis also identifies four successive stages in NW Greenland: (1) initial preglacial conditions, (2) glacial advance 1, (3) glacial retreat and interglacial conditions and (4) glacial advance 2 (current ice-sheet development). C/N and δ^{13} C data suggest that deglacial environments favored the development of tundra and taiga ecosystems. These two successive glacial fluctuations observed at NEEM are consistent with those identified from the Camp Century core basal sediments over the last 3 Ma. Further inland, GRIP and GISP2 summit sites have remained glaciated more continuously than the western margin, with less intense ice-substratum interactions than those observed at NEEM.

1. Introduction

Climate affects the volume and extent of the Greenland Ice Sheet (GrIS); yet our knowledge of climate's influence on Pleistocene history and environmental conditions prevailing during ice-sheet build-up remains fragmentary (e.g. Dutton and others, 2015; Westerhold and others, 2020). It is critical to better understand the sensitivity of the GrIS, and its ecosystems relative to different climate states as human-induced climate change increases in magnitude and duration. Our understanding of GrIS past history mostly relies on indirect archives, such as marine sediments (Larsen and others, 1994; de Vernal and Hillaire-Marcel, 2008; Bierman and others, 2016; Tripathi and Darby, 2018; Christ and others, 2020) or seismic surveys (e.g. Knutz and others, 2019) that allow insights about GrIS behavior over millions of years (Tripathi and Darby, 2018). Terrestrial archives are rare and discontinuous, including sediment deposits (e.g. Funder and others, 2001; Bennike and others, 2010; Corbett and others, 2021; Larsen and others, 2021), ice-core basal ice layer (BIL) debris and bedrock (e.g. Souchez and others, 1994; Verbeke and others, 2002; Willerslev and others, 2007; Bender and others, 2010; Bierman and others, 2016; Goossens and others, 2016; Schaefer and others, 2016; Yau and others, 2016a, 2016b; Christ and others, 2021). Evidence of past ecosystems comes from pollen, spores or fossils found in terrestrial or marine sediments (e.g. de Vernal and Mudie, 1989; Funder and others, 2001; Bennike and others, 2010) but also from the study of debris in the ice-core BIL (e.g. Willerslev and others, 2007; Christ and others, 2021).

BIL describes the bottom layer of the ice sequence present at the interface with underlying till and/or bedrock. These ice layers often bear debris from beneath the ice sheet. Majority of basal ice is thought to originate from the surface, and had been further diagenetically modified by processes operating at the bed (Knight, 1997). Some, however, like at the GRIP location, suggest a pre-ice-sheet origin, from local ice fields or permafrost (Souchez and others, 1994; Tison and others, 1998). The BIL material constitutes a unique and direct archive of sediments from Greenland's interior and represents a promising, yet under-utilized, archive of climate information. It is a scarce, but limited, continental archive that holds information about GrIS past behavior (Weis and others, 1997; Bierman and others, 2014; Schaefer and others, 2016), Greenland's past ecosystems (Willerslev and others, 2007; Christ and others, 2021), sub-ice-sheet geology (Fountain and others, 1981; Weis and others, 1997) and basal ice

© The Author(s), 2023. Published by Cambridge University Press on behalf of The International Glaciological Society. This is an Open Access article, distributed under the terms of the Creative Commons Attribution-NonCommercial-ShareAlike licence (<http://creativecommons.org/licenses/by-nc-sa/4.0/>), which permits non-commercial re-use, distribution, and reproduction in any medium, provided the same Creative Commons licence is used to distribute the re-used or adapted article and the original article is properly cited. The written permission of Cambridge University Press must be obtained prior to any commercial use.

[cambridge.org/jog](https://www.cambridge.org/jog)



processes (Tison and others, 1993, 1994, 1998; Souchez and others, 1994; Souchez and others, 2000; Verbeke and others, 2002; Souchez and others, 2006; de Angelis and others, 2013; Goossens and others, 2016). The study of its structure and geochemistry is a key to understanding ice-sheet behavior, as well as subglacial erosion and deposition as it offers a window into processes occurring at the ice-sheet bed (Knight, 1997).

Here, we examine the archive of BIL material from the NEEM ice core that was drilled in the north-western Greenland and is one of few GrIS cores that retrieved rock debris (Fig. 1). The structure and ice of the NEEM BIL were described and analyzed by Goossens and others (2016), but the debris was not specifically studied beyond its grain size distribution. The goal of this study is to gather as much information as possible from the material contained in the NEEM BIL, allowing us to characterize the potential sub-ice-sheet geology of the area, to widen the amount of data available for Greenland BIL material, and allow comparison with other ice cores. To do so, we present morphologic–microscopic, chemical and isotopic analyses of recovered grains to characterize the nature, origin and transport history of the sediment encountered in the NEEM basal ice. Along with geochemical analyses of meteoric ^{10}Be and organic nitrogen and carbon, this dataset assists with the identification and description of past ecosystems of the fluctuating glacial–interglacial paleoenvironment of northwestern Greenland. These new data are compared to those obtained from other Greenland deep ice core records (Willerslev and others, 2007; Bierman and others, 2014; Schaefer and others, 2016; Yau and others, 2016b; Christ and others, 2021).

2. Background: previous work on Greenland basal ice debris from ice cores

Debris-rich material in the BILs of Greenland is available in only few cores (Fig. 1): Camp Century, GISP2, NEEM and, in much smaller proportion, in GRIP and Dye-3 (Fig. 1; Tison and others, 2019). Only few studies have examined the BIL debris in Greenland ice cores to understand ice-sheet basal processes and Greenland subglacial geology.

Regarding subglacial processes, Whalley and Langway (1980) analyzed quartz grains from the subglacial sediment of the Camp Century ice core using scanning electron microscopy (SEM) to characterize grain shape and various microtextures to assess grain transport. They distinguished two grain categories: angular grains resulting from glacial grinding and well-rounded grains produced by aeolian transport, likely prior to ice-sheet build-up. Petrologic geochemical analyses of several clasts from the Camp Century subglacial sediment allowed documentation of the subglacial geology of northwestern Greenland (Fountain and others, 1981). The nature of the basal ice in the NEEM core has been well described by Goossens and others (2016), but information is still lacking about the nature and morphological characteristics of the debris. Significant spatial variability of the neodymium (ϵNd) and strontium ($^{87}\text{Sr}/^{86}\text{Sr}$) isotopic signatures was documented in Greenland from the analysis of bedrocks cropping out at the periphery of Greenland (Collerson and others, 1989; Weis and others, 1997), but also by analyzing moraines, cryoconites and dust sources from local Greenland soils (Nagatsuka and others, 2016; Simonsen and others, 2019). ϵNd and ($^{87}\text{Sr}/^{86}\text{Sr}$) of silt and clay particles from BIL of GISP2

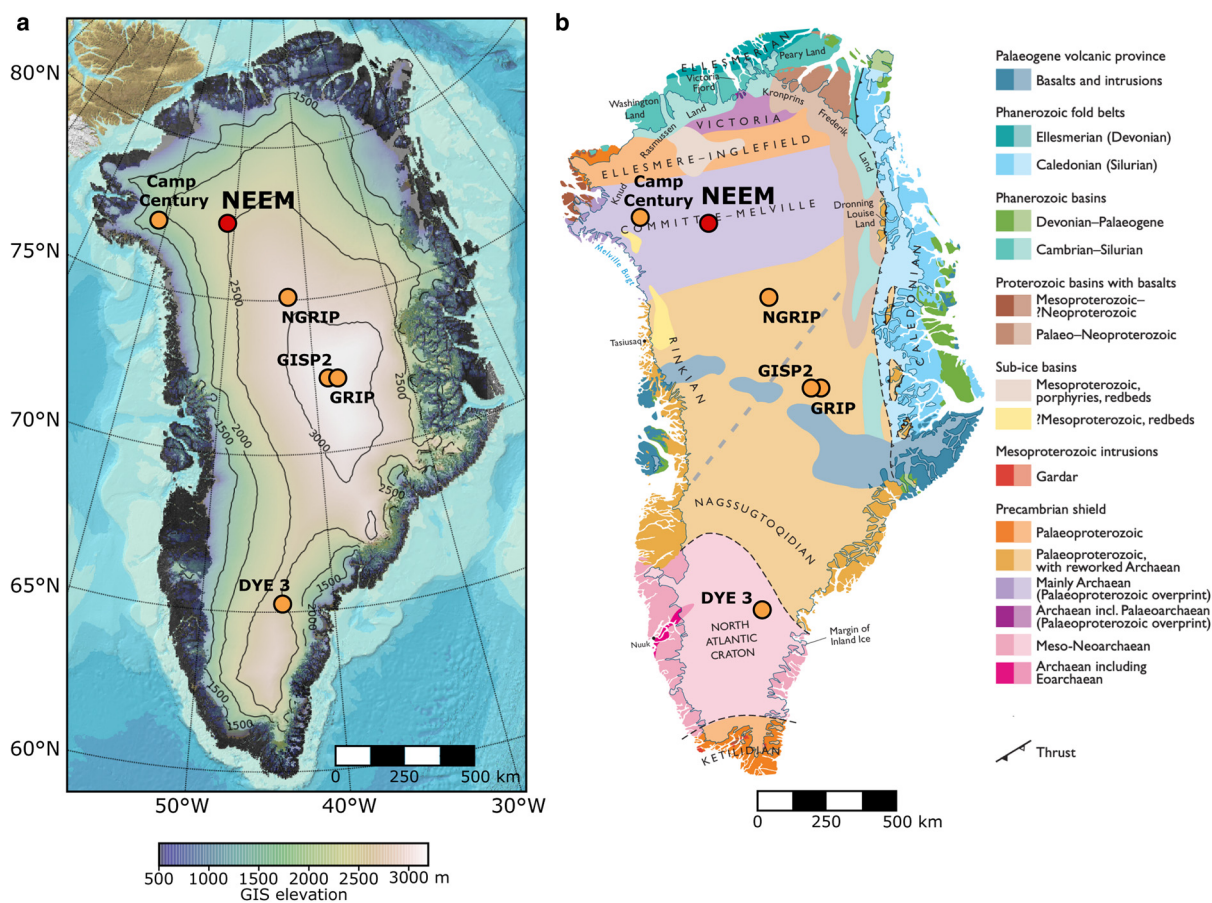


Figure 1. Overviews of Greenland with location of this study ice core NEEM (red dot) and others Greenlandic ice core referred to in the text (orange dots). Greenland map on the left (a) is from the Greenland Ice Sheet CCI project (composite product of Cryosat-2 elevation measurements and the 5 m DEM from the Polar Geospatial center). Geological map with interpretation of sub-ice bedrock on the right (b) is from Dawes (2009). Note that geological domains shown here are mainly extrapolated from coastal observations (darker colored areas in b).

and GRIP (Central Greenland) allowed Weis and others (1997) to identify the origin of the basal material in these two ice cores (Fig. 1b): local granitic bedrock for BIL sediments in GISP2, and subglacial till located above the GISP2 bedrock for BIL sediments in GRIP. These observations support the idea that lateral transport of basal sediment may have occurred, by lateral ice motion. Other ϵNd and ($^{87}\text{Sr}/^{86}\text{Sr}$) data from the upper Holocene and Pleistocene ice of Central Greenland suggested that the dust recorded in the upper ice section is very different from the local sources and was probably transported from Asian deserts (Bory and others, 2003a, 2003b). However, the ϵNd and ($^{87}\text{Sr}/^{86}\text{Sr}$) isotopic composition of the NEEM basal debris was still unknown.

Other investigations of ice core basal materials yield information about the past behavior and stability of the GrIS. In the south-central ice core DYE-3 and in GRIP (see Fig. 1 for locations), using DNA and amino acids of biomolecules from basal ice, Willerslev and others (2007) reconstructed the past ecosystem of Greenland. Those locations were probably forested and hosted insect colonies some time before the Last Interglacial (~130–116 ka). Analyzing cosmogenic atmospherically produced beryllium-10 (meteoric ^{10}Be), organic carbon and total nitrogen of sediments from the BIL of GISP2, Bierman and others (2014) suggested the long-term, multimillion year-long preservation of paleosols, likely from boreal regions and cryoturbated tundra, at the center of the GIS, suggesting a stability of the ice sheet and low subglacial erosion rates during most of the Pleistocene. These authors also proposed that the Greenland Summit (i.e. at location of GISP2) was continuously covered by ice over the Quaternary. Based on cosmogenic in situ produced beryllium-10 (^{10}Be) and aluminium-26 (^{26}Al) measured in the bedrock beneath the GISP2 ice core, Schaefer and others (2016) modeled hypothetical GIS fluctuation scenarios since 2.6 Ma and contrarily suggested that the GrIS may have near completely disappeared several times during the warmest and longest interglacial episodes of the Pleistocene. More recently, applying multiparametric analyses (SEM of grain coatings, in situ ^{10}Be and ^{26}Al , luminescence

dating, geochemical analyses and characterization of fossils plants and biomarkers) in basal ice sediments from the Camp Century ice core, Christ and others (2021) postulated at least two GrIS reductions in the northwestern Greenland over the last ~3 Ma, including the presence of a tundra ecosystem during an ice-free episode within the last 1.1 Ma.

3. Materials and methods

3.1. NEEM core and samples description

We studied samples from the BIL of the NEEM ice core (Fig. 1), a ~2544 m-long ice core drilled between 2008 and 2012 in north-west Greenland (77.45°N, 51.06°W). Despite being folded in its lower section, the NEEM ice core provides a near-continuous paleoclimatic archive for at least the past 130 ka, with evidence of the penultimate Glacial Period (MIS6, Dahl-Jensen and others, 2013). Below 2533.85 m depth, the core includes a 10 m sequence of debris-rich layers (Goossens and others, 2016). Analysis of the water-stable isotopes, ice fabrics, total gas content, debris weight and debris size distribution of BIL from NEEM identified different ice types: clear ice with specks, stratified debris-rich layers and ice containing dispersed debris (Goossens and others, 2016). The NEEM BIL has been interpreted as an ice–bedrock interface resulting from the incorporation of bedrock and till materials, as well as ice transformation processes occurring under a well-developed ice mass (Dahl-Jensen and others, 2013; Goossens and others, 2016). The NEEM basal section differs from that at GRIP, where the BIL is thought to be a pre-existing ice remnant that was covered by an advance of a growing ice sheet in central Greenland (Tison and others, 1994, 1998; Weis and others, 1997).

We first updated the initial log of the NEEM basal ice core (Goossens and others, 2016) by adding new macroscopical observations of the basal layers (Fig. 2a). We then provide a suite of new measurements focused on the debris material to decipher geological sources and better characterize the BIL environment and associated debris entrainment processes. We analyzed nine

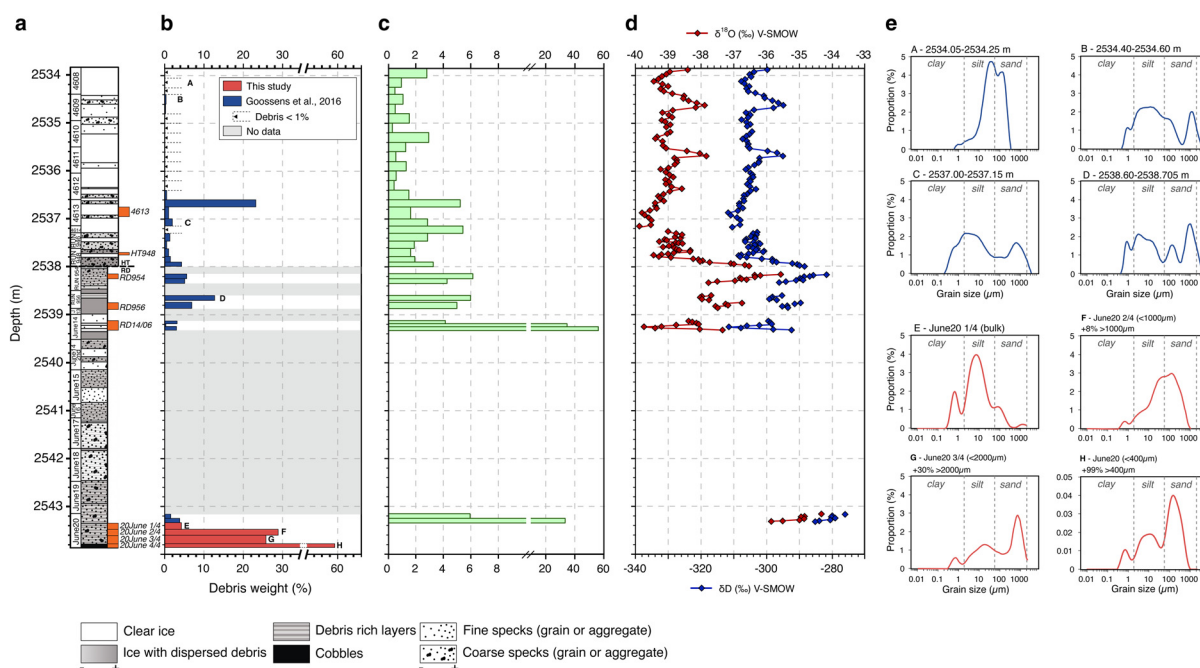


Figure 2. (a) Symbolic representation of the core stratigraphy. Names of the core bags are indicated on the left of the log. The orange bars represent the location of the samples used in this study, from top to bottom: 4613, HT948, RD954, RD956, RD14/06, 20 June 1/4, 20 June 2/4, 20 June 3/4, 20 June 4/4; (b) debris content in weight percentage (Goossens and others, 2016 – except for the red bars); (c) total gas content (Goossens and others, 2016); (d) $\delta^{18}\text{O}$ and δD (Goossens and others, 2016); (e) granulometric plots for eight samples (blue curves are from Goossens and others, 2016). Positions of the samples in the core are indicated by capital letters in (b). It should be noted that the scale of graph H is different.

different samples representative of different levels of the basal section of the ice core that were isolated after ice cutting, melting and drying (orange bars in Fig. 2a). These samples cover ~6 m of core, at depths from 2536.75 m (top) to 2543.785 m (bottom). The upper five samples (4613, HT948, RD954, RD956, RD14/06) were already melted and dried in the study by Goossens and others (2016), to report the debris weight content. The lower four samples (20 June 1/4, 2/4, 3/4, 4/4) were newly sampled for this study.

Below 2538 m depth, the drill head Hans Tausen (HT, 9.8 cm inner diameter) was changed for a purpose-built rockdrill head of 2.5 cm inner diameter. This was necessary to manage cutting through the increasing debris load but reduced the amount of available core material between 2537.990 and 2543.785 m (Fig. 2). The 2.5 cm diameter basal core limits the amount of available material, as a result not all the analyses presented in this study have been performed on all nine samples. The samples-analysis matrix is detailed in Table 1.

3.2. Additional sedimentological analyses: debris proportion and granulometry

To build on the initial results of Goossens and others (2016) and provide a better picture of the debris nature and abundance down to the bottom of the core (2543.785 m), we estimated the debris content and granulometry of the new samples. Each frozen subsample was first weighed at -20°C, then thawed and oven-dried at 50°C. The dried material was then weighed to calculate the weight percentage of debris in the ice. The sediments were then sieved using 75, 400 and 2000 µm sieves. Laser granulometry was performed on the size fraction <2000 µm at Université Libre de Bruxelles (ULB, Brussels, Belgium) using a *Malvern Mastersizer 3000* laser granulometer.

3.3. Mineralogical analyses

To characterize the sediments in the basal ice of the NEEM core, we used a multi-proxy analysis of the grains contained in the ice of the BIL. To investigate the diversity of mineralogy encountered in the basal sediments, the mineralogy of a few randomly selected grains (~2 mm) from samples RD954 ($n=10$) and 20 June 3/4 ($n=14$) was analyzed using a CAMECA SX100 electronic probe at Georessource Laboratory (Nancy, France). These grains were randomly hand-picked before being embedded into resin and polished.

3.4. Morphological analyses of sediment grains

To understand grain provenance and their transport history, we performed a morphometry analysis of sample grains (Cailleux

and Tricart, 1959; Mahaney, 2002; Woronko, 2016). For this, we first observed the selected samples with the light microscope, and we later used an SEM/EDS (scanning electron microscope/energy-dispersive spectrometer) approach to analyze grain morphology, composition and microtextures. Grain morphology and surface microfeatures can be interpreted to indicate different grain transport processes (glacial, fluvial, aeolian) and also reflect on their past and present environments, such as storage in soils (paleosols) or in ice, and in the presence of liquid water (Mahaney, 2002). This approach has been applied in multiple glacial contexts and has proven useful to derive information on grain history, paleoenvironment and paleoweathering conditions (Tison and others, 1993; Mahaney, 1995, 2002; Mahaney and others, 2013). A randomly selected and representative amount of grains (>100–300 µm sand-silt size grains) was observed using a JEOL JSM-6510 SEM at the Centre de Recherches Pétrographiques et Géochimiques (CRPG Nancy, France) for samples 4613 (<63, 63–125, >125 µm), HT948 (<63, 63–125, >125 µm), RD954 (<75, 75–250 µm), RD956 (<75, 75–250 µm), RD14/06 (<75, 75–250 µm), 20 June 1/4 (bulk), 20 June 2/4 (<75, 75–1000 µm), 20 June 3/4 (<75, 75–400 µm), 20 June 4/4 (<75, 75–400 µm). The chemical composition of selected key grains was determined with the EDS (energy-dispersive spectrometer) available on the same SEM instrument.

3.5. Geochemical analyses

3.5.1. ϵ Nd and $^{87}\text{Sr}/^{86}\text{Sr}$ analyses

To characterize the provenance of the silicate minerals in the NEEM BIL sediment and compare them with other Greenland records of aerial dust (Bory and others, 2003a, 2003b; Simonsen and others, 2019), glacial sediments (Nagatsuka and others, 2016) and bedrock (Collerson and others, 1989; Weis and others, 1997), we measured Sr and Nd isotopic ratios, as well as Rb and Sm, in the finest grain size (<63 or <75 µm, depending on the sample) of the samples RD954, RD956, RD14/06 and 20 June 1/4 to 20 June 4/4 at Laboratoire G-Time (Brussels, Belgium). About 100 mg of each sample was first digested using a mixture of concentrated sub-boiling HF and HNO₃ in the proportion 1:3. After 48 h on hot plate at 120°C, the supernatant was removed and the solid residue was further digested in a fresh mixture of 1:3 HF:HNO₃ in Parr high-pressure vessels for 48 h at 150°C. The dissolved samples were recombined with the supernatant and evaporated. Concentrated subboiled HCl was added at 120°C for 48 h. After evaporation, samples were re-dissolved in 2N HCl and two aliquots of 1% (in weight) each were taken for Sr isotope measurement and Rb/Sr measurement, and a 5% aliquot was taken for Sm-Nd spike. The rest was used for Nd isotope measurements.

Table 1. Details of the different analyses performed for each sample

Sample	Depth top-bottom (m)	Debris content	Granulometry	Microprobe	SEM/EDS	Carbon and nitrogen		Meteoric ^{10}Be		Strontium and neodymium
						CRPG	VUB	CRPG	UVM	
4613	2536.75–2536.95	–	–		X			X	X	
HT948	2537.72–2537.76	–	–		X	X		X	X	
RD954	2538.145–2538.245	–	–	X	X	X		X	X	X
RD956	2538.74–2538.87	–	–		X	X	X		X	X
RD14/06	2539.33–2539.53	–	–		X					X
20 June 1/4	2543.35–2543.485	X	X		X	X		X	X	X
20 June 2/4	2543.485–2543.61	X	X	X	X	X	X	X	X	X
20 June 3/4	2543.61–2543.785	X	X	X	X	X		X	X	X
20 June 4/4	2543.785–2543.84	X	X		X			X		X

‘–’ means that the analysis has been performed in (Goossens and others, 2016).

The Sr aliquot was purified using Sr.Spec resin by rinsing the matrix using 2N and 7N HNO₃ and collecting Sr with 0.05N HNO₃. The Sr cut was measured on the Nu Plasma 2 MC-ICP-MC at Laboratoire G-Time, ULB in dry mode using a DSN desolvator in 0.05N HNO₃. All values were corrected to the accepted value of NBS987 = 0.710248 (Weis and others, 2006). The USGS BHVO-2 standard yielded an ⁸⁷Sr/⁸⁶Sr of 0.703488 ± 0.000009 (2 SE) comparable with the accepted value of 0.703487 ± 0.000019 (Weis and others, 2006). The Rb/Sr ratio was directly measured on the ICP-MS Agilent 7700 by preparing both an elemental and a gravimetrically prepared ratio calibration curves, and using In as internal standard for monitoring possible drift. Each sample was measured three times and the RSD was better than 1%.

For Nd isotopes, the matrix was first removed by using 2 mL of cationic resin AG50-X8 200–400 mesh in 1.5N HCl, rare earth elements (REE) being collected in 6N HCl. Subsequently, Nd was purified from other REE using HDEHP resin with 0.16N HCl, Nd being collected with 0.27N HCl. The spiked aliquot followed the same procedure, except that Sm was collected further on the HDEHP resin by using 0.75N HCl. The Nd cut was measured on the Nu Plasma 2 MC-ICP-MC at Laboratoire G-Time, ULB in dry mode using a DSN desolvator in 0.05N HNO₃. All values were corrected to the accepted value of the Rennes standard of ¹⁴³Nd/¹⁴⁴Nd = 0.511961 (Chauvel and Blichert-Toft, 2001). USGS BHVO-2 standard yielded an ¹⁴³Nd/¹⁴⁴Nd of 0.512986 ± 0.000006 (2 SE), to be compared with the accepted value of 0.512984 ± 0.000011 (Weis and others, 2006). The spiked Nd and Sm were measured on the Nu Plasma 2 and the concentration was obtained by iterative calculation. Total procedural blanks yield <400 pg for Sr, <70 pg for Nd and <15 pg for Sm.

3.5.2. Organic geochemistry: C, N and δ¹³C

C and N concentrations, as well as the δ¹³C, provide clues about the origin, the nature and the degree of degradation of the organic material produced by the ecosystems prevailing during ice-free intervals (e.g. Bierman and others, 2014 and references therein). We measured total organic carbon (C), total nitrogen (N) and δ¹³C on the finest grain size (<63 or <75 μm, depending on the sample) of six samples to understand what surface material, including vegetation, from ice-free paleoenvironments was incorporated into the BIL by ice–substratum interactions. We analyzed the six samples that had sufficient amounts for these carbon nitrogen analyses.

One batch of carbon analyses was performed at VUB (Brussels, Belgium), with samples RD956 and 20 June 2/4. A second batch of carbon and nitrogen analyses was then performed at CRPG (Nancy, France), for the samples HT948, RD954, RD956, 20 June 1/4, 20 June 2/4, 20 June 3/4. This approach allows evaluation of the interlaboratory reproducibility.

In both labs, the determination of total carbon and nitrogen concentration, and the ¹³C/¹²C ratio of organic matter (hereafter referred in delta notation as δ¹³C vs V-PDB) were performed using online combustion coupled to an Elemental Analyzer – Isotope Ratio Mass Spectrometer (EA-IRMS). At the VUB, the measurements were performed on a EURO Elemental Analyzer (Eurovector, Italy) coupled with a Nu Horizon IRMS (Nu instruments, UK), with the temperature of the oven and the chromatographic column at 1030 and 80°C, respectively. At the CRPG, a Thermo Scientific Elemental Analyzer IsoLink IRMS System was used, with the temperature of the oven and the chromatographic column at 1020 and 70°C, respectively. At VUB, prior to analysis, the samples underwent a decarbonization process (i.e. contact with a 5% HCl solution and oven drying overnight) to which no response was observed. At CRPG, samples were not decarbonized based on the observations previously made at

VUB that lead to the conclusion that no carbonate was present. In both laboratories, samples were wrapped in tin capsules (~30 mg) before combustion. At VUB, C concentrations were calibrated using a sucrose internal standard. The international standard Low Organic Soil Standard OAS (C = 1.61 ± 0.09%w/w; N = 0.133 ± 0.023%w/w; δ¹³C = –26.66 ± 0.24‰) was included in the analysis and measured with a reproducibility of 0.5‰ (C). At CRPG, carbon isotopic composition was determined by comparison with two internal and two international standards routinely included during the analysis: (i) BFSd (C = 0.53 wt.%; δ¹³C = –21.5‰), (ii) CRPG_M2 (C = 0.408 wt.%; δ¹³C = –25.0‰), (iii) NBS22 (δ¹³C = –30.0‰) and (iv) USGS24 (δ¹³C = –16.1‰). Values are quoted in the delta notation (δ) in ‰ relative to V-PDB and the reproducibility was better than 0.2‰. The thermal conductivity detector signals calibrated with internal standards were used to calculate carbon and nitrogen concentrations: (i) BFSd (C = 0.53 wt.%), (ii) CRPG_M2 (C = 0.408 wt.%), (iii) Eurovector Synthetic Soil Mix #4 (C = 2.417 wt.%; N = 480 ppm), (iv) USGS AGV-1 (N = 28 ppm) and USGS G-2 (N = 34 ppm).

3.5.3. Meteoric ¹⁰Be

We measured meteoric ¹⁰Be (¹⁰Be_m) adsorbed on the sediment surface. ¹⁰Be_m is a cosmogenic nuclide produced in the atmosphere and deposited on the Earth's surface through precipitation and dry deposition. It partitions strongly to particle surfaces in soil and sediment (e.g. Pavich and others, 1984; Jungers and others, 2009; Graly and others, 2010). The ¹⁰Be_m proxy is used in soil science to provide chronological constraints on soil processes, evaluate weathering rates and provide clues on the origin of sediments (e.g. Jungers and others, 2009; Graly and others, 2010; Willenbring and von Blanckenburg, 2010; Wittmann and others, 2015). ¹⁰Be_m measured in materials from sub-ice-sheet environments records previous exposure of sediments during periods of deglaciation. Analyses of ¹⁰Be_m in GISP2 basal sediments were interpreted to infer paleosol exposure time (Bierman and others, 2014), while measurements of ¹⁰Be_m in periglacial sediments provided clues about nature and rate of subglacial processes (Graly and others, 2018). Here we test this approach on the basal sediments of the NEEM core, to better constrain the history of these debris. These data also allow us to discuss potential exchanges of ¹⁰Be_m between the embedded sediments in the BIL and the overlying clear ice of NEEM, in which ¹⁰Be_m was previously measured by Sturevik-Storm and others (2015).

¹⁰Be_m was extracted from the finest grain size (<63 or <75 μm, depending on the sample) of isolated and dried sediment (see section 2.2.1), following two procedures: (1) by KHF₂ total fusion of the sediments (4613, HT948, RD954, RD956, 20 June 1/4, 20 June 2/4 and 20 June 3/4) at the University of Vermont (Burlington, USA) and (2) by leaching of the sediment (4613, HT948, RD954, 20 June 1/4, 20 June 2/4, 20 June 3/4 and 20 June 4/4) at CRPG (Nancy, France). The first method (total fusion) extracts ¹⁰Be_m adsorbed on the grain surface as well as the in situ ¹⁰Be (¹⁰Be_i) component contained within the grains. The second procedure (leaching) allows the measurement of ¹⁰Be_m and ⁹Be adsorbed on the surface of the grains and the determination of the ¹⁰Be_i component after a final dissolution step. However, both approaches should yield similar results, since the adsorbed meteoric ¹⁰Be_m is several orders of magnitudes greater than the in situ component (e.g. Christ and others, 2021).

The extraction by KHF₂ fusion is based on the procedure of Stone (1998). Sample size ranged between 20 and 500 mg of dry sediment. We measured the mass of each sample and added ~1.3 g of a 304 ppm ⁹Be carrier solution, equivalent to ~400 μg of ⁹Be (2.03 × 10¹⁹ Be atoms). ¹⁰Be_m was extracted after fluxing of the sample by successive perchlorate and alkaline

precipitations. Final precipitates were dried using a 65°C hotplate and burned to turn into oxides before measurement of the $^{10}\text{Be}/^9\text{Be}$ ratio.

The extraction by leaching followed the chemical procedure first described by Bourlès and others (1989), updated and detailed in Simon and others (2016). $^{10}\text{Be}_m$ and ^9Be were leached from 6 to 100 mg of dry sediment using a 0.04 M hydroxylamine and 25% acetic acid solution at $90 \pm 5^\circ\text{C}$ for 6 h. After this step, we took a small aliquot of 2 mL of the resulting solution to measure the ^9Be concentration. About 0.25 g of the 2020 ± 80 ppm in-house ^9Be carrier solution PHENA (Puchol and others, 2017) was added to the remaining solution prior to the ^{10}Be extraction. ^{10}Be was finally extracted and purified by successive separations on anion- and cation-exchange resin columns and alkaline precipitations of $\text{Be}(\text{OH})_2$. The final deposits were then oxidized at 700°C for 1 h.

For both procedures, the final BeO oxides were mixed with Nb powder and loaded into nickel cathodes for AMS ^{10}Be measurements. All $^{10}\text{Be}/^9\text{Be}$ ratios were measured at the French national AMS facility ASTER (Arnold and others, 2010) at CEREGE (Aix-en-Provence, France). Measured $^{10}\text{Be}/^9\text{Be}$ ratios were calibrated against an in-house standard STD-11, assuming a $^{10}\text{Be}/^9\text{Be}$ ratio equal to $1.191 \pm 0.013 \times 10^{-11}$ (Braucher and others, 2015), equivalent to the KNSTD07 standardization (Nishiizumi and others, 2007). Analytical uncertainties of AMS measurements include counting statistics (internal reproducibility) and external reproducibility ($\sim 5\%$; Arnold and others, 2010) and blank correction. Uncertainties from chemical blanks were calculated for each batch (total fusion and leaching) based on the mean of two individual blanks. Blanks have ratios of $6.67 \pm 0.40 \times 10^{-15}$ (total fusion) and $1.14 \pm 0.30 \times 10^{-15}$ (leaching) (Table 2).

4. Results

4.1. Debris weight content and granulometry

Debris weight content for the four deepest samples (20 June 1/4, 20 June 2/4, 20 June 3/4, 20 June 4/4) varies between 4% (20 June 1/4) and 59% (20 June 4/4), with values around 25% for the two middle ones. 20 June 4/4 contains a pebble ($\sim 2 \times 1 \times 1.5$ cm) that accounts for most of its total volume. When considered with the samples from the BIL previously studied by Goossens and others (2016), the compiled observations display a first-order increase of the debris weight content with increasing depth (Fig. 2b). However, the presence of a few layers at $>10\%$ debris weight content (higher up in the sequence) sandwiched within the clear ice suggests shearing/folding processes of bottom material (Goossens and others, 2016).

Laser granulometry curves demonstrate a sharp increase of the coarser fraction at the boundary between the samples 20 June 1/4 (Fig. 2e-E) and 20 June 2/4 (Fig. 2e-F), reinforced by the presence of a pebble in sample 20 June 4/4. When compared to the curves of the samples from the BIL previously studied by Goossens and others (2016), the three deepest samples appear to be coarser than in the upper part of the core. The granulometry of sample 20 June 1/4 (Fig. 2e-E) is globally in agreement with the granulometry observed in the ice layer displaying the first dispersed debris at the top of the sequence (Fig. 2e-A). This observation also supports shearing/folding processes mixing horizons of different origins (Goossens and others, 2016).

4.2. Mineralogical characterization of the sediments

Mineralogical analysis of RD954 and 20 June 3/4 by electronic probe showed the presence of quartz, plagioclase and K-feldspar (Fig. 3). A rough counting based on binocular observations

indicates that these three mineral species represent a large majority of the grains (80–90%). The analysis also reveals the presence of muscovite, carbonate, clay, amphibole and garnet, in lesser proportions (10–20%) (Fig. 3).

4.3. SEM imagery: characterization of the main features at the grain surfaces

The SEM imagery of grain microtextures and EDS chemical analysis of nine different core sample groups are the basis of our detailed interpretations. Figures 4 and 5 present a selection of SEM photos showing the diversity of grain morphology and the main microfeatures encountered in the different samples. Figure 4 displays upper samples of the core section: groups 4613, HT948, RD954, RD956 and RD14/06, while Figure 5 shows the lower samples: groups 20 June 1/4, 20 June 2/4, 20 June 3/4 and 20 June 4/4. A larger collection of other pictures is available in Supplementary material.

Our SEM observations of the grain textures show that, in all these samples, there is a mix of weathered (dissolution-affected and coated, Figs 4a, d, f, 5f) grains and other physically abraded grains (by ice-rock or grain to grain contact, Figs 5b, c, f), with an increase in the proportion of fresh grains toward the bottom of the core (Figs 4, 5). Indeed, microtextures indicating glacial transport and glacial crushing (triangular-shaped grains, with subparallel and conchoidal fractures, uplifted plates, grooves (Figs 4b–f, 5b, c, f) and weathering features (dissolution microfeatures, coating; Figs 4b, d, e)) were found at all depths in the BIL, with a less intense weathering toward the bottom of the core (Fig. 5e).

No round grains were observed and nearly all grains have angular to subangular shapes, the latter being dominant among the analyzed grains. Numerous triangle-shaped grains were imaged (Fig. 5f), a form that possibly is a product of variable pressure release or shearing, from stick-slip pressure dynamics (Mahaney, 1995). In all samples, weathered grains have numerous microfeatures indicative of physical abrasion, including uplifted plates (Fig. 4a), strong-to-light dissolution microfeatures of varying size (Figs 4f, 5d) thin-to-thick coatings (Figs 4b, d, e), subparallel fractures (Figs 4d, 5d) and grooves (Fig. 5a). Very angular grains with fresh fractures and evidence of physical abrasion were also observed, with greater abundance at the bottom of the core (Figs 4a, 5a–c, f). Mineralized wood/pith fragments were also present at the bottom of the core (Fig. 5a).

A grain of unknown composition (probably feldspar), shown in Figure 4c, displays important minor uplifted plates, with multiple dissolution features and adhering particles, along with thick coating (Smalley, 1966). Such features indicate a progression from a pre-weathered environment (favoring dissolution and grain coatings) to active glaciation yielding the adhering particles, from glacial grinding. Figures 4a–d, f, 5b and d display a variety of angular to very angular quartz grains in different mechanical/weathering states presenting multiple microfeatures such as uplifted plates, dissolution microfeatures, subparallel fractures, grooves (striae) and v-shaped percussion cracks. While scarce, the v-shaped percussion cracks suggest water action, possibly from moulin or basal meltwater transport (Mahaney, 2002). In particular, the grain in Figure 4b is covered by a thick coating ($\sim 2 \mu\text{m}$ deduced from the SEM instrument operating at 20 keV) of secondary minerals, containing mainly Fe, with Na, Mg, Al, K and Ca. This coating, shown in brown in Figure 4b, locally covers adhering particles (arrow A) and is intercepted by fresh fractures within the grain (arrow B), which undoubtedly occurred after the weathering event. A similar observation is made on the grain shown in Figure 4e. Thus, we have identified grains carrying mechanical/weathering/scars indicative of successive stages of weathering, glacial crushing and transport.

Table 2. Samples and blanks details relative to the meteoric ¹⁰Be measurements at UVM (A) and CRPG (B)

A – UVM				B – CRPG				
Sample	Grain size (µm)	Mass (g)	Carrier (µg ⁹ Be)	¹⁰ Be/ ⁹ Be (×10 ⁻¹⁵)	1σ (×10 ⁻¹⁵)	[¹⁰ Be] (×10 ⁶ at.g ⁻¹)	1σ (×10 ⁶ at.g ⁻¹)	
4613	<63	0.023	392	11.03	0.87	3.85	0.96	
HT948	<63	0.043	392	9.42	0.85	1.30	0.51	
RD954	<63	0.045	392	8.88	0.77	1.00	0.46	
RD956	<75	0.111	392	23.36	1.41	3.05	0.29	
20 June 1/4	<63	0.197	392	21.71	1.20	1.55	0.14	
20 June 2/4	<75	0.505	392	39.98	1.63	1.34	0.07	
20 June 3/4	<75	0.125	392	18.37	1.15	1.90	0.22	
BLK			392	6.39	0.62			
BLK X			392	6.95	0.69			
Sample	Grain size (µm)	Mass (g)	Carrier (mg ⁹ Be)	Natural ⁹ Be (×10 ¹⁵ at)	¹⁰ Be/ ⁹ Be (×10 ⁻¹⁵)	1σ (×10 ⁻¹⁵)	[¹⁰ Be] (×10 ⁶ at.g ⁻¹)	1σ (×10 ⁶ at.g ⁻¹)
4613	<63	0.007	0.2582	1.420	2.12	0.28	5.27	1.80
HT948	<63	0.049	0.2548	1.496	4.03	0.36	2.10	0.30
RD954	<63	0.044	0.2649	1.378	4.20	0.39	2.63	0.37
20 June 1/4	<63	0.093	0.2663	2.016	5.36	0.42	1.71	0.19
20 June 2/4 A	<75	0.106	0.2607	3.143	4.80	0.40	1.27	0.15
20 June 2/4 B	<75	0.046	0.2579	0.952	3.12	0.37	1.55	0.33
20 June 2/4 C	<75	0.094	0.2595	1.134	4.94	0.40	1.48	0.17
20 June 3/4	<75	0.098	0.251	2.466	7.04	0.59	2.13	0.22
20 June 4/4	<75	0.006	0.2594	0.039	3.29	0.32	13.17	2.30
BLC1			0.2593		1.35	0.22		
BLC2			0.2513		0.93	0.18		

For 20 June 2/4, we used the mean of the three CRPG replicates. ¹⁰Be/⁹Be ratios are uncorrected from the chemical blank. ¹⁰Be atom in the samples is calculated from the corresponding ratios and corrected from that of the mean of the chemical blanks at UVM and CRPG apart. [¹⁰Be] is calculated from the blank corrected number of ¹⁰Be atoms.

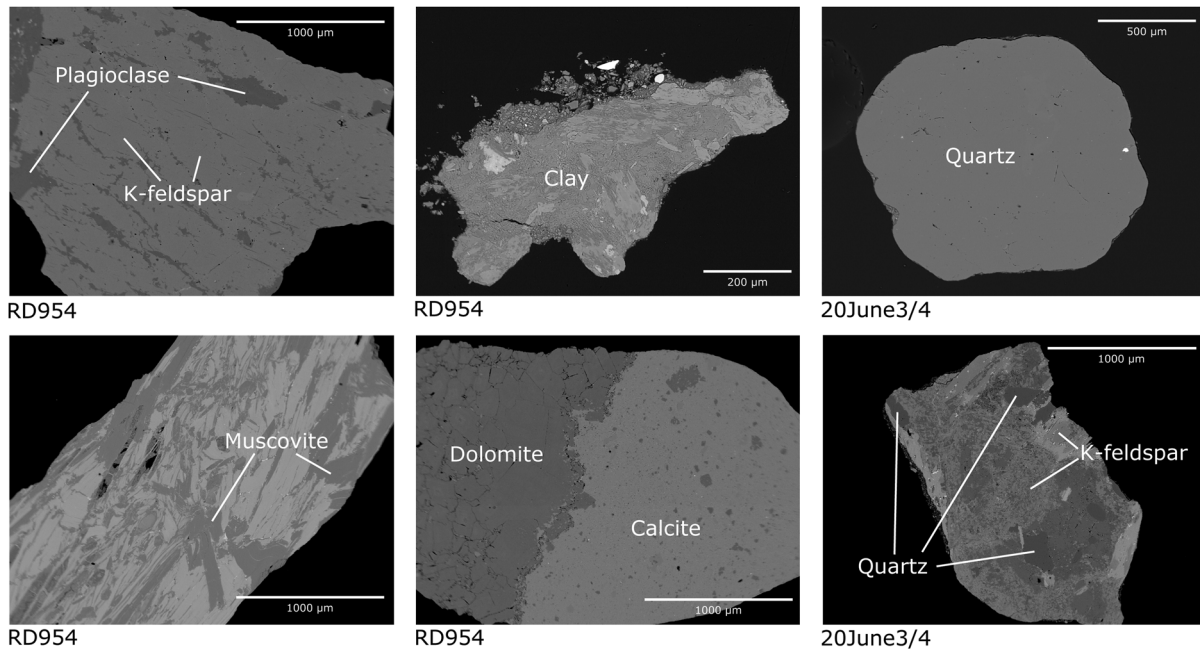


Figure 3. Backscatter electron (BSE) images of grains from RD954 and 20 June 3/4 analyzed by electronic probe with determined mineralogy.

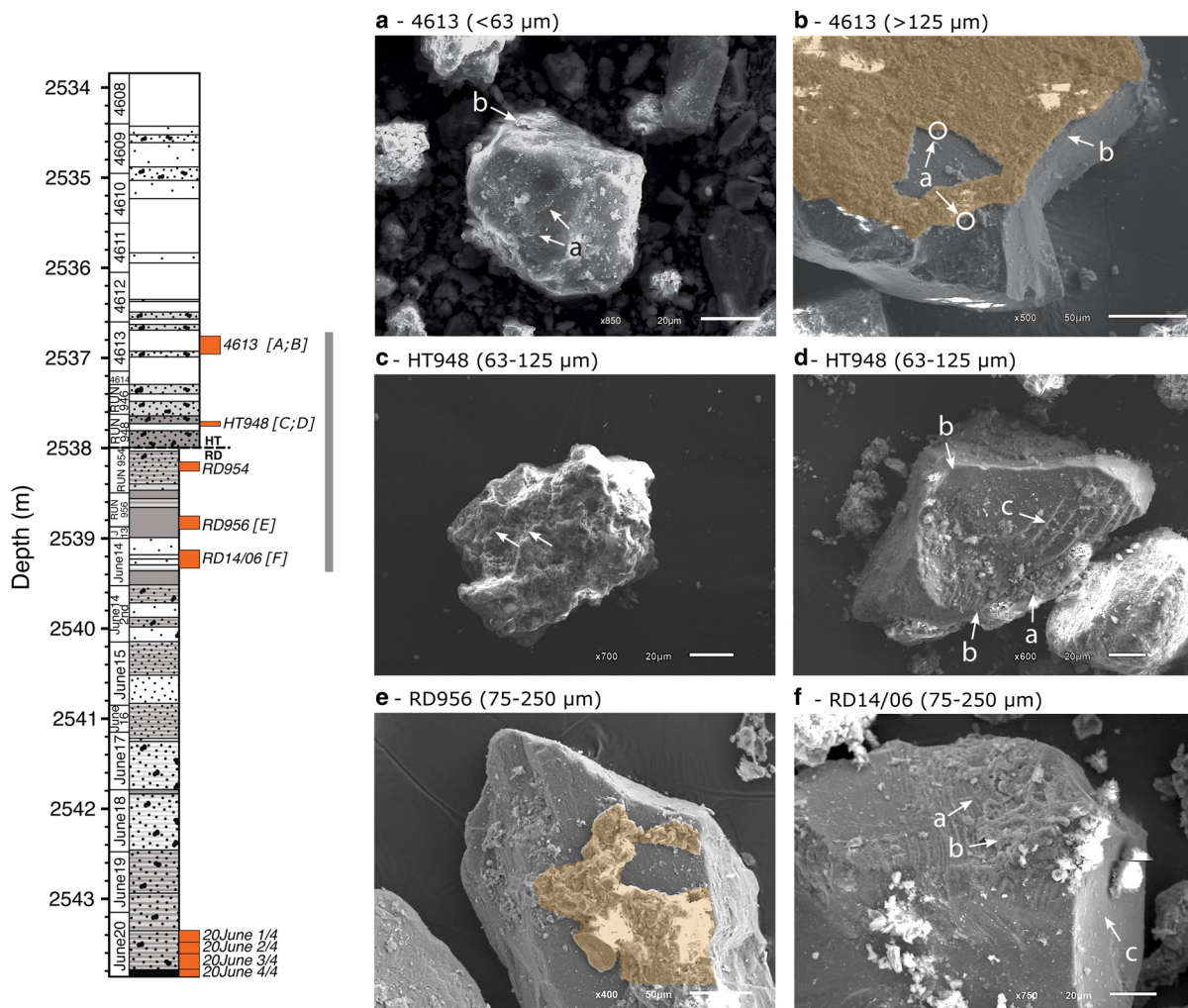


Figure 4. SEM imagery from key grains in NEEEM upper samples (4613; HT948; RD954, RD956 and RD14/06): (a) Coarse silt size quartz with numerous uplifted plates (arrows A) and weathered particles pack (arrow B) in upper lower left large groove. (b) Quartz in the medium sand fraction with a thick (~2 μm) coating masking a grid of protruding particles (arrows A), which may represent a long weathering period. The mineral coating is intercepted by fresh fractures within the grain (arrow B). (c) Coarse silt of unknown composition with large-scale grooves, and dissolution microfeatures carrying thick coatings on grain surface and adhering particles. Weathered staircase fractures (arrows) may represent ‘chattermarks’ (Folk, 1975). (d) Coarse silt with secondary mineral coatings (arrow A), rounded edges and different angularities (arrows B). Posterior sub-parallel to conchoidal fractures varying in weathered state, with adhering particles (arrows C). (e) Mechanically altered feldspathic grain with thick and partial coating in places. Abraded striations center-left could relate to reworking, one glaciation to another. (f) Quartz grain with numerous subparallel weathered linear/conchoidal subparallel fractures (arrow A), partially covered by secondary mineral coating (arrow B). A latter fresh fracture crosscut the coating (arrow C).

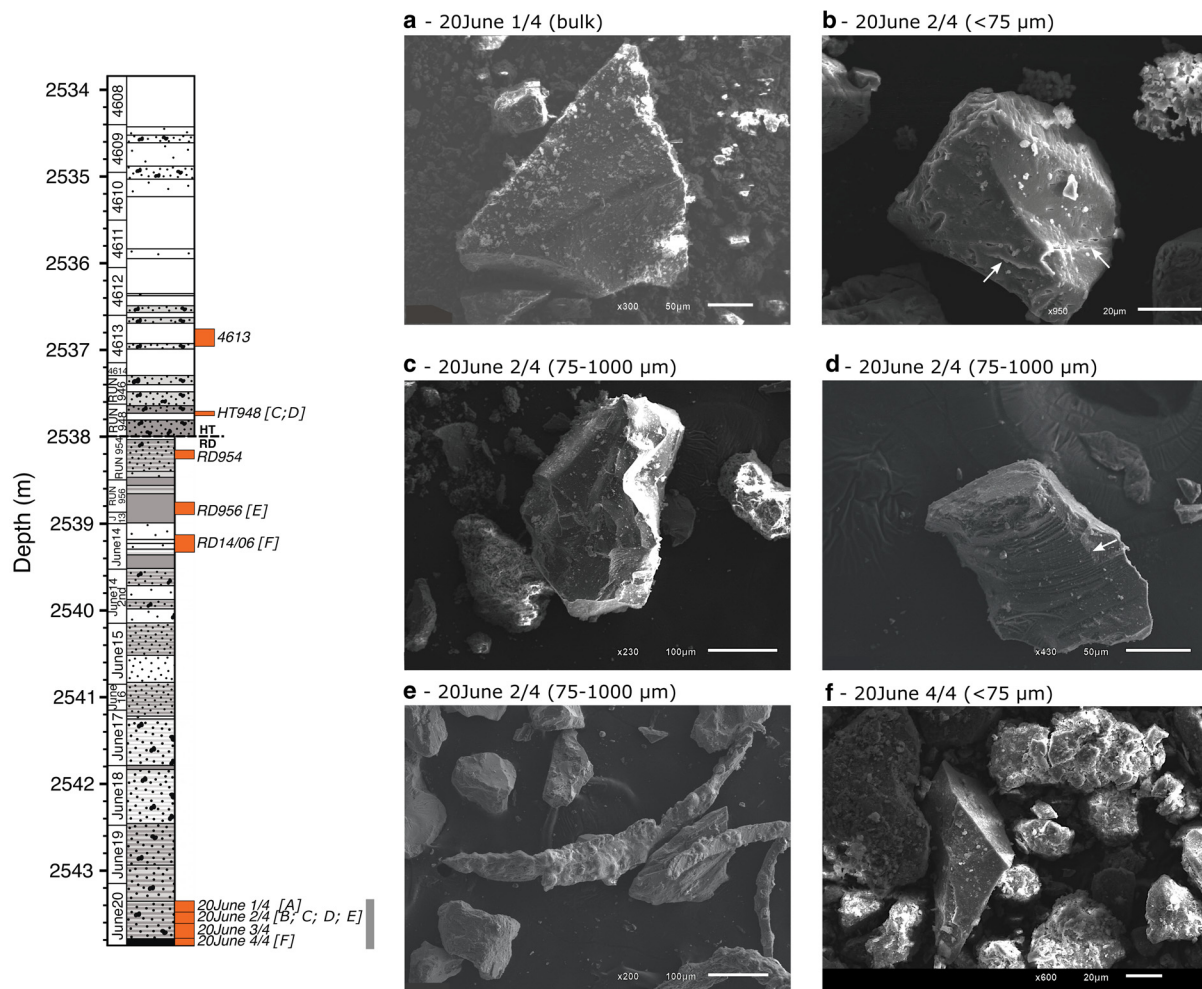


Figure 5. SEM imagery from key grains in NEEM lower samples (20 June 1/4; 20 June 2/4; 20 June 3/4 and 20 June 4/4): (a) Angular quartz with adhering silt particles, minimal coating and a deep, wide groove in center. (b) Angular quartz of coarse silt-fine sand transition size with weathered uplifted plates (arrows), minor dissolution microfeatures, Fe rims on uplifted mineral skin (suggests glacial release followed by weathering), angular fragments of fine silt size, with striations fragmented with light tones suggesting Fe coatings. Some cavities may be weathered v-shaped percussion fractures indicative of water movement. (c) Well-tumbled quartz grain with very sharp edges paired with abraded rounded forms, very little weathering and many adhering particles. (d) Angular quartz with large-scale multiple skin fractures inset with subparallel fractures, grooves/striations (upper-younger/center-lower older), and adhering particles, surrounded by angular silt particles, and reasonably fresh fracture face (top) suggesting bedrock release. (e) Wood/pith fragments (center right and lower right) with encrustations consisting of mineral fragments with coatings of Fe oxides and possible clay minerals of unknown composition. Nodal complexes may contain fossil microbial communities. Angular grains (center right and upper left) are striated with large grooves. Surrounding mix of grains are all angular. (f) Triangle-shaped quartz coated with adhering particles nested with finer grains of unknown composition showing variable charging and heavy coatings. Fracture face (center) reflects bedrock release.

The grain in [Figure 4d](#) is quartz with secondary mineral coatings (arrow A), rounded edges and different angularities (arrow B). The exposed internal part of the grain displays subparallel to conchoidal fractures in variable weathered states, with adhering particles (arrow C). Weathered subparallel fractures (arrow A) are also visible on the surface of the grain in [Figure 4f](#), partially covered by a secondary mineral coating (arrow B) and adhering particles. For almost all grains, fresh-appearing adhering particles are present on the surface of specimens thought to be the result of multiple glaciations.

In contrast, some grains, notably those from the lower-most part of the core, show very few signs of weathering, but have various fractures, grooves and microfeatures due to glacial transport ([Figs 5a, c, f](#)). The signs of weathering on the grain in [Figure 5f](#) (center left) suggest a sojourn in ice free of weathering events since bedrock release. [Figure 5d](#) displays a grain with fresh fracture, subparallel fractures and striations (see arrow), all comprising damage that are characteristic of bedrock release followed by grain-to-grain contact during glacial crushing processes. Also,

[Figures 5c and f](#) present very angular quartz grains with sharp edges and few adhering particles, with fresh surfaces that display no sign of weathering. Finally, we also observed few mineralized wood fragments with visible nodal complexes ([Fig. 5e](#)) that are coated with Fe oxides. The fact these fragments are mineralized is deduced from the observation that this material sinks in water. Such plant debris was only found in the sample 20 June 2/4.

4.4. Strontium and neodymium isotopic composition

Strontium and neodymium were measured in seven samples: RD954, RD956, RD14/06, 20 June 1/4, 20 June 2/4, 20 June 3/4 and 20 June 4/4. Results are presented in [Table 3](#) and [Figure 6](#). Measured $^{87}\text{Sr}/^{86}\text{Sr}$ ratios are tightly clustered and range between 0.750745 (20 June 4/4) and 0.761530 (20 June 3/4) ([Table 3](#) and [Fig. 6](#)). $\epsilon^{143}\text{Nd}$ range from -32.54 (RD956) to -29.42 (20 June 3/4). The two lower-most samples have the highest $\epsilon^{143}\text{Nd}$ values, while the others are statistically undistinguishable.

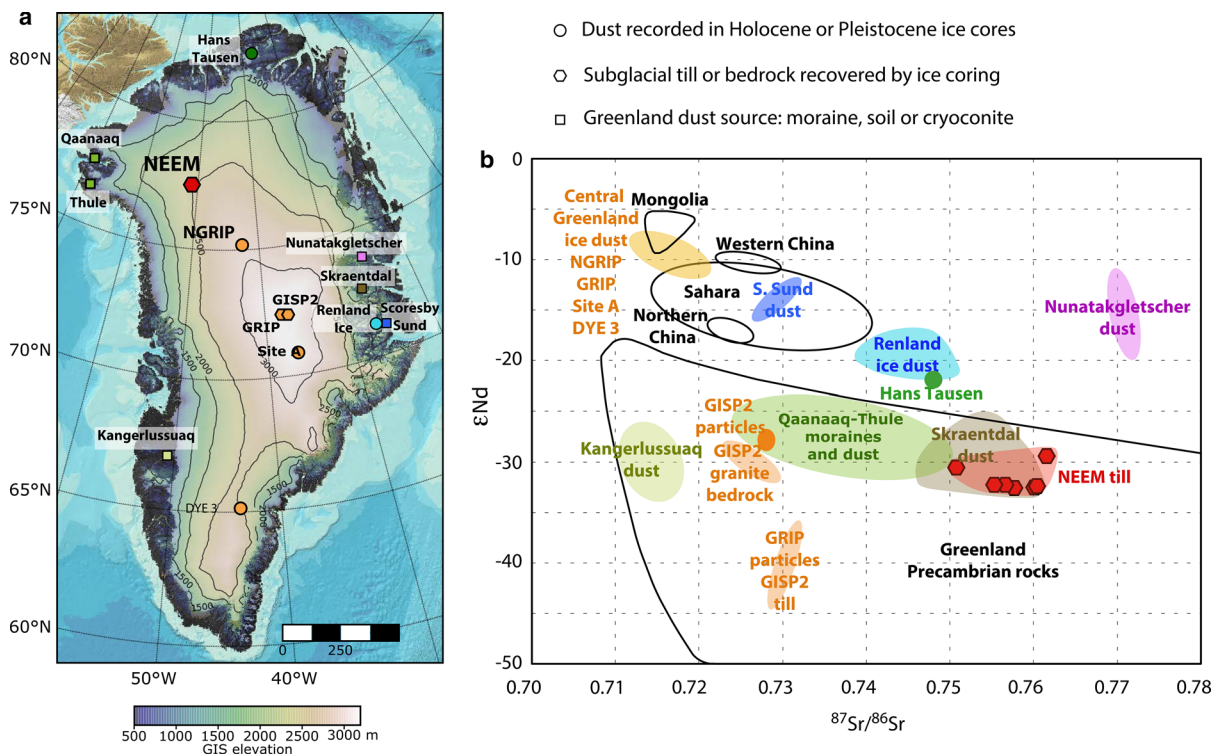


Figure 6. $^{87}Sr/^{86}Sr$ and ϵ_{Nd} isotopic signatures of Greenland rocks, tills, dust sources and dust recovered from drilled ice. NEEM basal tills (red polygons; this study) are compared to signatures of particles from the basal ice of GISP2 and GRIP and subglacial till material from GISP2 (dark orange; Weis and others, 1997). All these basal tills belong to the Precambrian rock domain defined by the data of Collerson and others (1989), as well as moraines and cryoconites from the western Greenland (Qaanaaq, Thule and Kangerlussuaq; light green squares; Nagatsuka and others, 2016). Dust sources from the eastern Greenland (Nunatakletscher, pink square; scores by Sund, blue square; Simonsen and others, 2019) belong to another domain, as well as the dust recovered in the Renland (light blue circle) and Hans Tausen (dark green circle) Holocene ice (Bory and others, 2003a, 2003b). Finally, the dust recovered from the Pleistocene and Holocene ice of the Central Greenland ice cores, namely NorthGRIP, GRIP, Site A, DYE 3 (orange circles) are distinct from these Greenland rock sources and are more probably from Asian sources (data from Biscaye and others, 1997; Svensson and others, 2000; Bory and others, 2002, 2003a, 2003b; Simonsen and others, 2019). All these isotopic ratios are reported as measured and were not corrected for the radioactive decay of ^{147}Sm and ^{87}Rb .

the other samples, regardless of the methods, have $^{10}Be_m$ concentrations an order of magnitude lower and range between $(1.00 \pm 0.40) \times 10^6$ (RD954) and $(5.50 \pm 1.65) \times 10^6$ at/g (4613). Apart from the fact that the highest concentration is observed in the lower-most sample of the core, there is no noticeable trend in $^{10}Be_m$ concentration with depth.

5. Discussion

The new data reported here add to previous knowledge of Greenland, its bedrock and interactions of the surface and solid Earth with the ice sheet. The data allow us to improve our understanding on three important topics: first, we constrain the debris nature and province to establish whether basal material was

derived from local rock; second, SEM imagery of grain textures and meteoric ^{10}Be provide clues about ice dynamics and erosional processes at the base of the GrIS, and occurrence of past ice-free conditions; finally, the geochemical analysis of the organic matter (N and C) provides clues about the nature of ecosystems during these ice-free conditions, and also about preservation of organic material in these BILs.

5.1 Rock source of the NEEM basal ice layers and implications for the whole of Greenland

Geochemical and mineralogical observations on the NEEM basal debris provide important clues about the provenance of debris in the BIL. These data show a strong similarity with the rocks

Table 4. Carbon and nitrogen concentrations, values of C/N ratio and $\delta^{13}C$ from analysis at CRPG (A) and VUB (B)

A – CRPG										
Sample	Number of replicates	Grain size (μm)	[N] (ppm)	2σ	[C] (wt%)	2σ	C/N	2σ	$\delta^{13}C$	2σ
HT948	1	<63	341	10	0.81	0.04	23.8	1.4	-26.13	0.18
RD954	1	<63	191	30	0.84	0.04	44.1	7.4	-27.41	0.19
RD956	3	<75	125	20	0.87	0.04	69.8	11.9	-27.06	0.21
June 20 1/4	4	<63	190	31	6.61	0.39	347.6	60.8	-30.62	0.23
June 20 2/4	7	<75	67	14	0.21	0.02	31.6	7.1	-25.32	0.27
June 20 3/4	4	<75	136	7	0.60	0.03	43.9	3.2	-22.43	0.33
B – VUB										
Sample	Number of replicates	Grain size (μm)	[C] (wt%)	2σ	$\delta^{13}C$	2σ				
RD956	3	<75	0.76	0.02	-28.39	0.23				
June 20 2/4	9	<75	0.17	0.02	-26.94	1.83				

The number of replicates for each sample is indicated in bracket after the sample name. Uncertainties of the C and N concentrations correspond to the internal and external uncertainties.

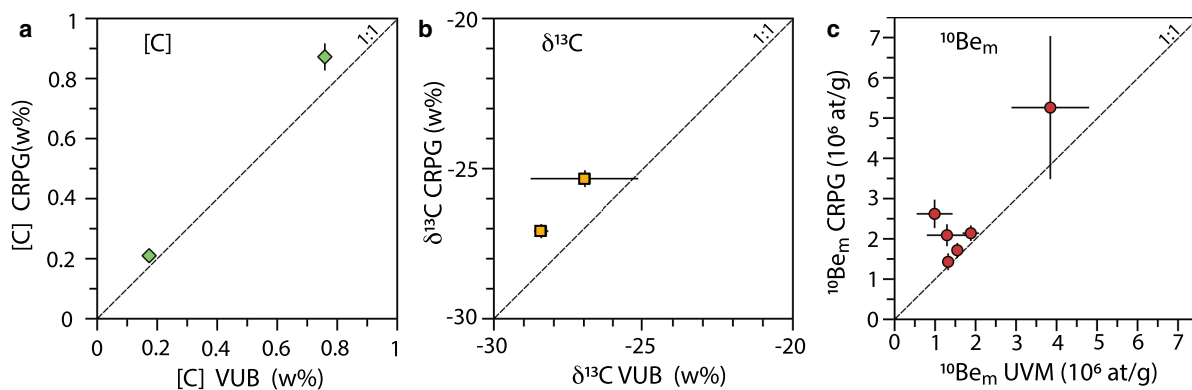


Figure 7. Interlaboratory comparison of [C], $\delta^{13}\text{C}$ and meteoric ^{10}Be measured in NEEM basal ice sediments: CRPG and VUB for [C] (green diamonds) and $\delta^{13}\text{C}$ (green squares) (samples RD956 and 20 June 2/4) and CRPG and UVM for meteoric ^{10}Be (red circles) (samples 4613, HT948, RD954, 20 June 1, 20 June 2 and 20 June 3). 2σ uncertainties are represented for [C] and $\delta^{13}\text{C}$, 1σ uncertainties for meteoric ^{10}Be . When not visible, uncertainties are less than the symbol size.

outcropping in northwestern Greenland, but also with local dust sources of the east coast. Although the NEEM core did not retrieve local bedrock, the principle of parsimony implies that this observation favors a rather local origin for the NEEM basal material.

First, it is important to discuss the potential transport distance of the basal ice material considering the present characteristics of the GIS dynamics. Given the NEEM core is located on an ice divide of the GIS today (Fig. 1), the basal debris found at NEEM probably underwent less lateral transport than other locations affected by much faster ice motions (e.g. <https://eo4society.esa.int/2021/07/01/a-breakthrough-in-the-quality-of-sentinel-1-ice-velocity-products/>). However, given that the NEEM ice surface is at a lower altitude compared to the Greenland summit (where the GRIP and GISP2 cores are located), the ice motion along this divide is not null, and there is still a potential for BIL (and debris) transport from regions located between the summit and NEEM (Dahl-Jensen and others, 2013). Modeling of ice particle trajectories showed that the Eemian ice originated from a few hundred kilometers upstream of

NEEM (Fig. 1a in Dahl-Jensen and others, 2013). In the NEEM core, the Eemian ice stands ~100 m above the debris-rich BIL; considering the horizontal ice velocity decrease with depth and the ice particle trajectories modeled by Dahl-Jensen and others (2013), the total displacement of the NEEM sediment from its source area is probably <200 km. This number should be considered with caution since ice dynamics may have changed during the Pleistocene.

Second, the mineral assemblages found in NEEM are typical of the Precambrian geological formations that crop out on the northwest Greenland coast. According to the geological map interpolated from coastal outcrops, the NEEM site probably belongs to the Committee-Melville Archean belt observed on the NW coast that is largely dominated by mixed-gneiss complexes (Fig. 1b; Dawes, 2009). Isotopic Sr and Nd data provide complementary observations that support this conclusion. The measurement of the father isotopes ^{147}Sm and ^{87}Rb in these samples permit to tentatively derive Sm-Nd and Rb-Sr isochrones: the seven samples yield overdispersed isochrones (errorchrons), with mean standard weighted deviation significantly larger than 1

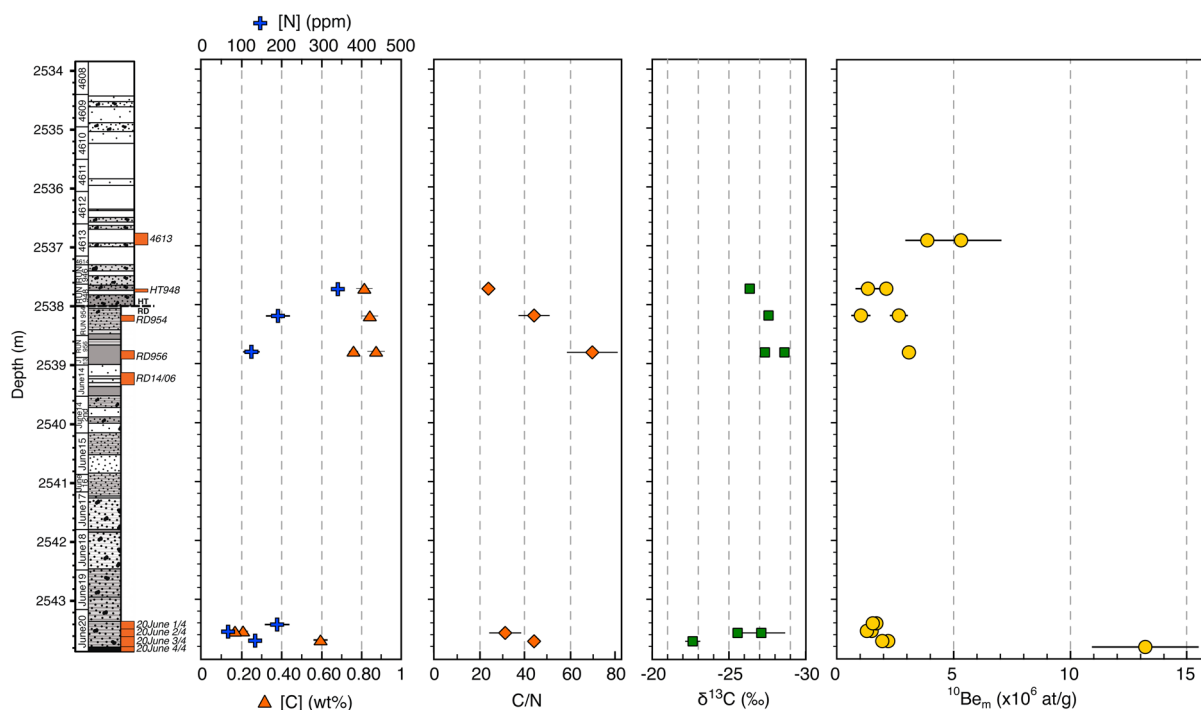


Figure 8. Geochemical data obtained on the NEEM basal sediments with regard to the log of the core: C/N ratio, $\delta^{13}\text{C}$ and meteoric ^{10}Be . When not visible, uncertainties are less than the symbol size.

(close to 100), indicating that this tills material probably result from the mixing of minerals having heterogeneous ages. Despite the existence of these heterogeneities, we can however report the apparent ages of these two errorchrons: our dataset yields ages of 2.3 ± 0.6 and 2.3 ± 1.1 Ga for the Rb-Sr and Sm-Nd systems, respectively. Such values are compatible, within uncertainties, to the Archean and Early Proterozoic eons and the ages obtained from the same isotopic systems in western and central Greenland (Collerson and others, 1989; Weis and others, 1997).

Although heterogeneities in Sm and Rb may modify the initial $\epsilon^{143}\text{Nd}$ and $^{87}\text{Sr}/^{86}\text{Sr}$ of the rock sources, several studies that documented the Sr and Nd isotopic signatures of Greenland rock did not necessarily apply this radioactive decay correction. Hence, for comparison with other Sr and Nd dataset measured in rocks, till and dust from other Greenland areas, we plotted our ϵNd and $^{87}\text{Sr}/^{86}\text{Sr}$ NEEM data along with the other records, without performing any correction for the radioactive decay of ^{147}Sm and ^{87}Rb (Fig. 6). In this diagram, $^{87}\text{Sr}/^{86}\text{Sr}$ and $\epsilon^{143}\text{Nd}$ isotopic signatures of the six NEEM basal sediments globally agree with the broad range signatures of the Precambrian gneiss and granite from terrains cropping out in northwest Greenland and Labrador (Collerson and others, 1989; Weis and others, 1997). The Sr and Nd isotopic compositions of the NEEM debris also overlap with those of moraines and cryoconite dusts measured in the nearby western edge of the GrIS, in Thule and Qaanaq (Nagatsuka and others, 2016), as well with the dust sources from the Skreantdal area, located in the Eastern Coast (Simonsen and others, 2019) (Fig. 6). The $^{87}\text{Sr}/^{86}\text{Sr}$ and $\epsilon^{143}\text{Nd}$ signatures of these NEEM tills are however clearly distinct from several dust sources from the East Greenland coast (Fig. 6), and also from subglacial material retrieved in the GISP2 and GRIP ice cores (Central Greenland – Figs 1, 6). These distinct Sr and Nd isotopic signature indicates that the basal debris of NEEM and Central Greenland are derived from different rock types. This observation is consistent with the subglacial geological limits inferred from the interpolation of terrains outcropping on the island's margins (Figs 1, 6): GISP2 and GRIP are expected to be located on Paleoproterozoic terrains that outcrop along 50% of the Central Western Coast, while the NEEM site is presumed to belong to the extrapolated position of the Committee-Melville Archean belt that outcrops along the NW coast (Fig. 1; Kirkland and others, 2009).

Finally, it is worth noting that this new Nd and Sr isotopic dataset reported for the NEEM basal debris is clearly different from those of dust embedded in younger Pleistocene and Holocene ice of Central (NorthGRIP, GRIP, Site A) and Southern Greenland (DYIE-3) (Fig. 6; data from Biscaye and others, 1997; Svensson and others, 2000; Bory and others, 2002, 2003a, 2003b). This observation strengthens the previously established conclusion that rules out a local Greenland origin for the dust embedded in the Pleistocene and Holocene ice of the GrIS: dust that has 'rained' above the GrIS during the Pleistocene originates from Asian deserts (e.g. Biscaye and others, 1997; Simonsen and others, 2019).

5.2. Grains imagery: SEM/EDS textural constraints on the GrIS dynamic

Our SEM analyses of grain textures (Figs 4, 5) provide information that permit constraining multi-scale processes, and notably the chronology of past waning and waxing of the GrIS. The presence of high-relief features such as grooves, numerous uplifted plates and subparallel to conchoidal fractures indicates that grains were affected by stick-slip pressures possibly up to ~ 200 bars (Barcilon and Macayeal, 1993; Mahaney, 2002) and transported by ice that was probably >1000 m thick (Mahaney, 1995). In the NEEM BIL sediment, we did not find any rounded grains or

signs of abrasion fatigue indicative of previous aeolian or fluvial transport and abrasion (Mahaney, 2002), in contrast to the observations previously made at Camp Century core (Whalley and Langway, 1980). This suggests that these features have never been developed or have been erased by subsequent glacial erosion. Goossens and others (2016) discarded an aeolian origin of the sediment based on debris size distributions through the basal core, but this does not preclude aeolian delivery to surfaces undergoing weathering prior to glaciation. The lack of abrasion features and any aeolian-induced shock melting from grain-to-grain collisions in SEM observations reinforces this conclusion. Even if uplifted plates and arcuate cracks may sometimes be observed in loess, the majority of the observed features and microtextures of the NEEM grains are not compatible with aeolian transport. Moreover, the coarse grain sizes of sediments at the bottom of the ice core (Fig. 2) are not likely to have been transported by air. Although it is possible that grains were transported via fluvial or subglacial meltwater prior to their incorporation into the ice, the majority of grain surface features observed by SEM indicate that these grains were extracted from bedrock, transported and reshaped by glacial erosion and abrasion (Figs 4, 5).

Despite this significant glacial imprint, not all grains have the same appearance and, hence, they do not share the same history. The heavy weathered coatings, intersected by more recent abraded faces on some grains, hold a weathering history prior to the final ice abrasion (Figs 4b, d–f). The thickness and aspect of these alteration coatings suggest formation in a preexisting soil (paleosol) environment that developed prior to sediment incorporation into the ice, where grains were later mechanically abraded and crushed. Furthermore, the presence of fossil wood in one of the bottom samples (Fig. 5e) indicates that the previous vegetation in these soils were mixed with glacial sediment that contained poorly weathered grains. This observation suggests that the BIL layer has probably incorporated some of a weathered paleosol and mixed it with less weathered sediments that were initially located deeper in the paleo-regolith in the vicinity of bedrock. Plant material, diatoms, fungi, microbes and insect fossils are present in the basal sediment of the Camp Century Greenland core (Harwood, 1986; Christ and others, 2021) and even in Antarctic paleosols (Mahaney and others, 2001; Lewis and others, 2008; Hart and others, 2011; Mahaney, 2015; Mahaney and Schwartz, 2021). These are clues indicative of warmer climatic conditions conducive to weathering and soil morphogenesis.

Our observations showed that some features cross-cut or were superimposed on other preexisting features of these grains (e.g. Figs 4b, d, f). Hence, some grains can be considered as mineralogical 'palimpsests' recording successive geomorphological and glacial histories. In these grains, the weathered aspect and the chemical coating deposited over glacial features indicates that chemical weathering occurred after an initial glacial crushing step. Glacial crushing post-dates all these previous features in several grains (Figs 4b, e, f). Such relationships are key because they permit us to reconstruct the succession of events and propose a broad scale history of the GrIS fluctuations: (i) initial weathering of grains in ice-free conditions, (ii) glacial abrasion, crushing and transport due to an earlier GrIS advance, (iii) weathering with the presence of liquid water, probably during ice-free conditions resulting from a significant retreat of the GrIS, (iv) glacial abrasion and transport that occurred during glacial readvance leading to the modern configuration of the GrIS (Figs 4b, d, f).

Although all grains did not record all of these three events, the majority of the observed features are compatible with a scenario involving two glacial events separated by a period of ice-free conditions. The numerous adhering particles observed on almost all grains (Figs 4, 5) were probably produced and deposited during the second, more recent glacial episode, while the majority of

the weathering features had been acquired by water circulation and grain dissolution/precipitation in a deglaciated soil (paleosol) environment. However, secondary low-intensity weathering might also have occurred after the incorporation of grains into the ice with ongoing melting/refreezing processes (Goossens and others, 2016). Such chemical weathering may happen under an active ice sheet when grains were in contact with meltwater and thus dominated by the incongruent dissolution of silicate (Urrea and others, 2019). However, such subglacial weathering was probably not intense enough to produce weathering features and the thickest coating (up to 10 μm) observed on some grains (Fig. 4) (Mahaney, 2002). Hence, even if subglacial weathering may have occurred, a deglaciation phase that led to prolonged sub-aerial conditions can be considered as the most probable scenario.

Some grains show less evidence of weathering but have numerous glacial transport microfeatures, notably in the bottom section of the core (Figs 5a, c, d). Fresh fractures indicating grain-to-grain contact (Fig. 5d) suggest recent incorporation into the ice from bedrock and a transportation time shorter than the weathered grains previously described in the upper sections. This type of debris is only observed in the samples at the bottom of the ice core (20 June 1/4 to 20 June 4/4) while the weathered-coated grains are found in all samples.

Together, these observations suggest two origins of debris found in the BIL. Some debris originated from a weathered substrate (probably the preglacial-paleosol) that was transported in the ice, where grains were modeled by abrasion/fracturing, followed again by weathering (most probably during a deglacial episode), and later incorporated into the ice. Other debris are sourced from the local substrate directly underneath the ice with little transport and shorter residence time, yielding to sharp edges and limited weathering. This second type of less-weathered debris is more abundant in the deepest section of the core, which suggests that the mixing and transportation is less efficient in the vicinity of the ice/substratum interface. Also, the sediment at the top of the BIL (above 20 June 1/4) has a much finer granulometry compared to the material found at the very bottom (under 20 June 2/4), suggesting a potential size sorting effect during the shearing process of grain entrapment and transport within the ice (Tison and others, 1993).

5.3. Significance of sediment-hosted meteoric ^{10}Be in the NEEM silty ice

Measured $^{10}\text{Be}_m$ concentrations in NEEM sediments (between ~ 1 and $\sim 10 \times 10^6$ at.g^{-1}) are one to more than two orders of

magnitude less than those measured in the basal sediments of GISP2 (10^7 to 10^8 at.g^{-1} , Bierman and others, 2014) (Fig. 9). Measured $^{10}\text{Be}_m$ concentrations at NEEM are of the same order of magnitude as those measured in Greenland glaciofluvial sediments (Nelson and others, 2014) and in glacial marine diamict offshore of northwestern Greenland that was derived from erosion of the island (Christ and others, 2020) (Fig. 9). This similarity suggests that $^{10}\text{Be}_m$ concentrations under much of the ice sheet are relatively low and that concentrations as high as those measured at GISP2 and in a small number of more marginal silty ice samples (Graly and others, 2018) are unusual. Such high concentrations of $^{10}\text{Be}_m$ could represent samples derived from pre-glacial landscapes that remain preserved below the ice sheet or from areas exposed during interglacial periods when ice was absent for long periods of time.

We suspect that the low concentrations of $^{10}\text{Be}_m$ at NEEM reflect effective erosion and/or short periods of interglacial exposure. Short periods of exposure limit the input of $^{10}\text{Be}_m$ from the atmosphere whereas erosion removes the uppermost parts of the soil and regolith profiles that often contain the highest concentrations of $^{10}\text{Be}_m$ (Graly and others, 2010). In permafrost, most $^{10}\text{Be}_m$ is contained in the shallow active layer which is typically no more than 1–2 m deep, and sometimes much less (see profiles in Bierman and others, 2014 and Diaz and others, 2021). Thus, glacial erosion of surface materials can remove large portions of the $^{10}\text{Be}_m$ inventory from the landscape. Considering the mixed grain populations observed using SEM analysis, it is probable that the sediment samples from which we extracted $^{10}\text{Be}_m$ are a mixture of two endmembers: some were freshly mined from bedrock by glacial abrasion and plucking while others were reworked from interglacial or pre-glacial paleosols. Fresh grains from unweathered substratum carry very low concentrations of $^{10}\text{Be}_m$ ($<10^4$ at.g^{-1}) whereas the grains sourced from upper soil layers are likely to carry much greater concentrations of $^{10}\text{Be}_m$ in their grain coatings ($>10^6$ at.g^{-1}) (Fig. 9).

There are uncertainties inherent to extracting $^{10}\text{Be}_m$ from silty ice, but we do not believe these explain the low concentrations of $^{10}\text{Be}_m$ measured in NEEM samples. $^{10}\text{Be}_m$ concentrations measured in the NEEM clear ice is $\sim 10^4$ $\text{at.g}_{\text{ice}}^{-1}$ (Sturevik-Storm and others, 2015), two orders of magnitude below the concentrations reported here in the NEEM basal sediments. Although $^{10}\text{Be}_m$ exchange between ice and debris still need to be better understood (e.g. Baumgartner and others, 1997; Willerslev and others, 2007), $^{10}\text{Be}_m$ may be leached in acid liquid water conditions encountered in some soils (with $\text{pH} < 4$). The pH of refrozen basal water from the nearby NorthGRIP core is between 5.0 and 5.3 (Christner and others, 2012), a priori too high for mobilization of $^{10}\text{Be}_m$.

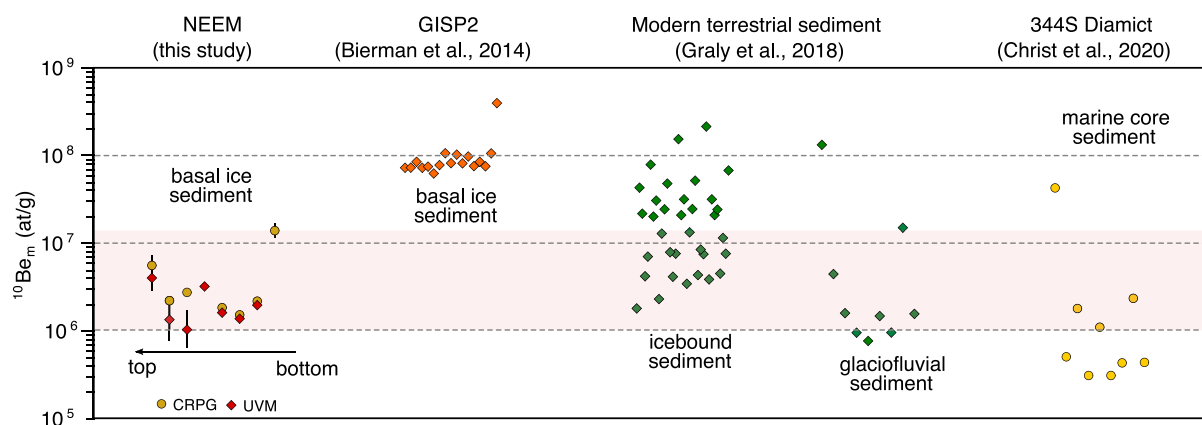


Figure 9. Comparison between meteoric ^{10}Be measured in NEEM basal sediment (this study) and other Greenland archives: GISP2 basal ice sediments (Bierman and others, 2014), modern terrestrial sediments (Graly and others, 2018) and marine core diamict (Christ and others, 2020). The latter are decay corrected for 1.9 Ma. Data from this study are presented from top to bottom, any order was not kept for the other studies. When not visible, uncertainties are less than the symbol size. Red boxes underline the range of the data from this study.

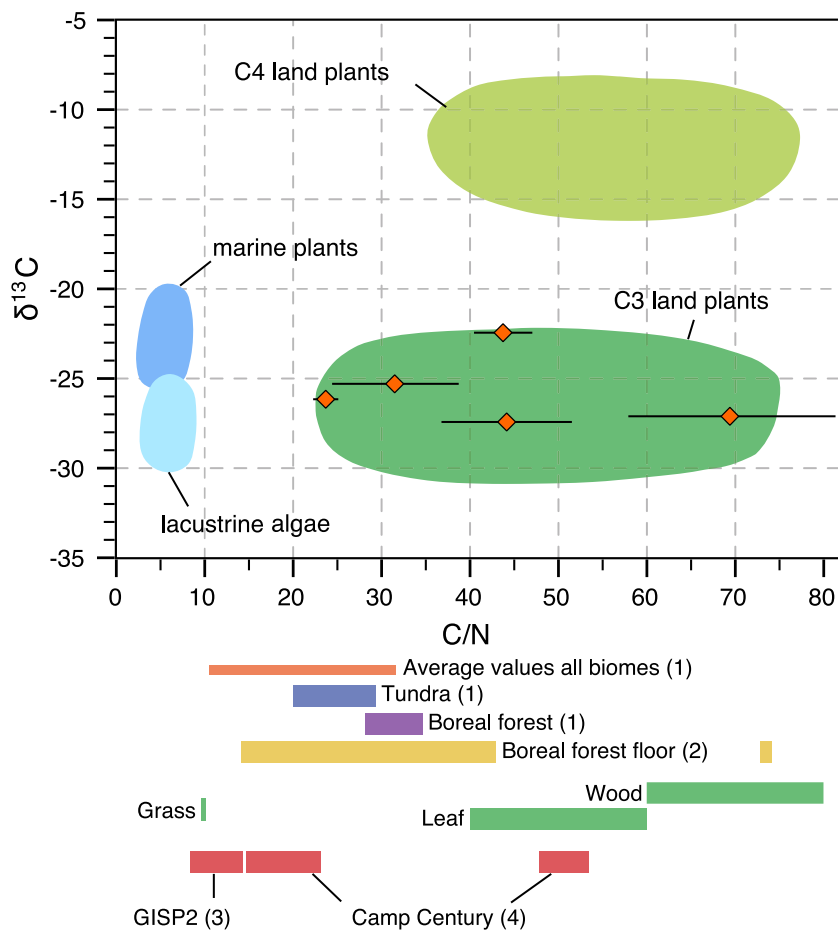


Figure 10. Distinctive source combinations of C/N ratio and $\delta^{13}\text{C}$ (from Meyers, 1994) and data measured in the NEEM basal sediments (orange symbols). Range of C/N ratios for all biomes taken together, tundra and boreal forest ecosystems, boreal forest floor, in turf, leaf and wood and in GISP2 and Camp Century basal sediments. References: (1) = Xu and others (2013), (2) Marty and others (2017) and references therein, (3) = Bierman and others (2014), (4) = Christ and others (2021). When not visible, uncertainties are smaller than the symbol size.

Additionally, the GISP2 subglacial material Bierman and others (2014) and ice-bound sediment samples of Graly and others (2018) were analyzed following a similar extraction procedure of removing silt from ice by melting. The GISP2 samples were more than 99% ice as were many of the Graly and others (2018) samples. The extraction of $^{10}\text{Be}_m$ from GISP2 silty ice (Bierman and others, 2014) and subglacial ice-bound silt and sand material (Graly and others, 2018) did not lead to a reduction of the $^{10}\text{Be}_m$ concentration to the level observed at NEEM. This reasoning leads us to believe that the NEEM $^{10}\text{Be}_m$ data we report here are robust and indicative of active erosion of the bed below and near NEEM over at least two glacial cycles. This inference is consistent with other data we present in this paper as well as the observation that basal temperature at NEEM is -2.4°C (Goossens and others, 2016) not far below the melting point of the local bed (-1.3°C ; MacGregor and others, 2015). It is reasonable to conclude that ice at NEEM was warm-based and erosive at some point in the past.

5.4. Paleoenvironment during previous deglaciation periods

C/N ratios of the sediments of the NEEM BIL range between 20 and 70. Some of these values are significantly higher than the average values of the organic material found in developed soils (10–30; Xu and others, 2013), and in Holocene-age tundra soils of northern Siberia (10–40; Ernakovich and others, 2015). In temperate regions, C/N ratios are known to reflect the degree of degradation of the organic matter and to decrease with depth (e.g. Callesen and others, 2007; Hugelius and others, 2010). In this framework, the C/N ratios measured in the NEEM sediments suggest that they originate from the upper layer (0–50 cm) of an

immature soil. The reason for soil to be poorly developed could be a short lifetime or a cold environment that would have prevented the organic matter from being degraded, and so that the C/N ratio has remained high (Oelbermann and Voroney, 2007; Ernakovich and others, 2015).

The NEEM C/N ratios agree quite well with the ratios of raw and non-degraded elements of continental higher plants, such as leaf and wood (Fig. 10), suggesting that this organic material is pristine and not degraded. These C/N ratios are also consistent with remains of boreal forest and tundra (Fig. 10), and in particular those of the boreal forest floor that can be as high (up to 40) as those measured in half of the NEEM basal sediments (Callesen and others, 2007; Marty and others, 2017). A boreal forest or tundra environment is moreover consistent with the $\delta^{13}\text{C}$ NEEM data (that range between -22 and -27‰) and is compatible with C3 land plants (Fig. 10; Meyers, 1994). Finally, paleosol conditions have also been evidenced by the coatings on debris surfaces and wood fossils found among the debris of the BIL (Fig. 5e). It is probable that these grain microfeatures formed synchronously with the development of vegetation during preglacial time or in an interglacial warm period.

The upper C/N value measured in the NEEM basal debris (~ 70) is compatible with one sample of woody tissue (60–80) recovered in the Camp Century subglacial sediment (Christ and others, 2021), and both are significantly higher than the C/N ratios (~ 10) measured in silty ice from GISP2 (Fig. 10; Bierman and others, 2016). Moreover, our data cover a large range (20–70) compared to the C/N ratios from the BIL of the GISP2 ice core that are more tightly clustered around 10 (Bierman and others, 2014). This discrepancy could be due to a difference in the maturity of the organic material and the paleosols from

which it is derived both. Indeed, the hypothesis of Bierman and others (2014) is that the GISP2 basal material corresponds to a well-developed soil, much more mature than the one observed at NEEM or, to a lesser degree, at Camp Century. This interpretation is also in agreement with the highest $^{10}\text{Be}_m$ concentrations measured at GISP2 that are interpreted as indicative of a well-preserved non-eroded paleosol (section 5.3).

If a mature soil did exist at NEEM, it seems to have been eroded and removed by early glacial advances, prior to the current ice-sheet expansion, in agreement with the succession of events determined from our grain morphology analysis. Given the location of GISP2 near the ice-sheet summit, where ice flow is almost null, the basal ice at GISP2 has likely been more stable than the ice at the NEEM location. Only a few tens of kilometers away from GISP2, BIL from the GRIP core contains elevated concentrations of biogenic gases (CO_2 and CH_4) and organic acids sourced from a local periglacial environment that developed prior to the full ice-sheet build-up (Tison and others, 1998; Souchez and others, 2006). Our SEM analysis of grain features at NEEM indicates the occurrence of (at least) two ice-free episodes and two glacial advances at NEEM that agrees with the two ice-free episodes recorded in the Camp Century subglacial sediment (Christ and others, 2021). The near-null ice velocity at GISP2 might have preserved the mature soil/paleosol developed before the last glaciation build-up (Bierman and others, 2014) that probably occurred 1 Ma ago (Yau and others, 2016a). In agreement with this scenario, gas composition trends in the southern distal core of Dye-3 indicate significant ice motion at this southern distal location (Fig. 1; Verbeke and others, 2002), while the record is much more stable at the GRIP location, at the GrIS summit (Souchez and others, 1995).

Finally, the C and N data in the NEEM material are consistent with a tundra or taiga paleo-ecosystem, an observation that is consistent with similar analyses of ice core basal materials in Camp Century (Christ and others, 2021), with ancient DNA from Dye-3 silty ice (Willerslev and others, 2007), and with fossils preserved in preglacial sediments (e.g. Funder and others, 1985, 2001; Drucker and others, 2010). The fossil wood fragments found here (Fig. 5e) also bear similarity to fossils found in the basal section of Camp Century (Christ and others, 2021).

6. Conclusions: past fluctuations of the GrIS at NEEM

Based on this multi-proxy analysis of the NEEM basal ice debris, we propose a history of the BIL debris with four successive stages: (1) initial preglacial conditions of uncertain duration for weathering/soil/paleosol genesis, (2) glacial advance 1, (3) glacial retreat and interglacial conditions with onset of weathering and (4) glacial advance 2 (current ice-sheet development).

According to Goossens and others (2016), the discrete debris layers visible higher up in the NEEM sequence result from shearing-in/folding of material from a layer of frozen sediments situated on top of bedrock. Our new data allow us to go further in the interpretation of the ice-sheet dynamics at the NEEM location (see schematic process timeline in Fig. 11). SEM-identified microfeatures are the primary data on which we base this interpretation. Indeed, the relationship between weathering (coatings) and glacial abrasion on grains suggests at least four successive stages of ice-sheet comings and goings. This interpretation is supported by C and N concentrations, $\delta^{13}\text{C}$ and $^{10}\text{Be}_m$ data:

(1) *Initial stage: preglacial conditions.* The presence of weathered grains in the BIL is consistent with the presence of a soil/paleosol layer developed on the local substrate. Although there is no control of the age of organic material found in the NEEM BIL, wood fossils, C/N ratios and $\delta^{13}\text{C}$ data are

consistent with tundra and/or boreal forest vegetation covering the landscape at that time (Fig. 11a).

- (2) *Glacial advance 1.* This first glacial advance not only eroded the weathered soil surface, but also mixed pre-glacial material with more deeply carved and exhumed fresh bedrock (yellow dots in Fig. 11b). This material had then probably been fractured and abraded by glacial plucking, and by transportation with grain-to-grain collisions in flowing ice (Fig. 11b). This scenario of deep (>1 m) regolith exhumation is also attested by the low $^{10}\text{Be}_m$ concentrations ($\sim 10^6$ atoms/g) measured in the NEEM BIL debris (Fig. 9). We suspect mixing diluted near-surface sediment containing higher $^{10}\text{Be}_m$ from weathered grains.
- (3) *Glacial retreat and interglacial conditions.* Ice retreat led to the deposition of debris contained into the BIL as till (Fig. 11c). The most compelling evidence for this ice-free episode is SEM/EDS observations that show thick secondary mineral coatings formed at the surface of some previously crushed grains, which we interpret as subaerial weathering conditions (Fig. 11). Moreover, a soil probably developed on top of this till, with tundra and/or boreal forest vegetation growth according to the C/N and $\delta^{13}\text{C}$ data.
- (4) *Glacial advance 2 (current ice-sheet development).* The development of the current ice sheet remobilized and incorporated previously weathered debris into the current BIL sequence (brown dots in Fig. 11d) and previously deposited till (yellow dots in Fig. 11d). This stage is supported by SEM analysis, showing the presence of freshly abraded grains, with fractures intersecting more weathered and coated grain surfaces (Figs 4, 11). The till and paleosol sources were once again mixed with fresh and less weathered bedrock materials, that have lower $^{10}\text{Be}_m$ concentration (orange dots in Fig. 11d), as supported by the $^{10}\text{Be}_m$ vs depth profile (Fig. 8, with the exception of the outlier bottom sample 20 June 4/4). It is worth noting that this mixing was apparently more efficient in the top section of the NEEM BIL, than at the very bottom, where crushed grains from fresh bedrock are dominant.

$^{87}\text{Sr}/^{86}\text{Sr}$ and $\epsilon^{143}\text{Nd}$ analyses of NEEM basal debris show that this material is very different from dust sources recorded in the Holocene and Early Pleistocene ice (e.g. Bory and others, 2003a, 2003b). The specific signature of the NEEM basal debris (Fig. 6) strongly suggests that this material is derived from a rather local bedrock source that probably experienced <200 km lateral transportation (Dahl-Jensen and others, 2013). The source of NEEM rock debris is probably the Committee-Melville Archean belt, which crops out on the northwest coast of Greenland (Figs 1, 6). These geochemical data also provide new insights about bedrock heterogeneities of the Greenland island, and may be useful for studies tracking sediment provenances in marine records (e.g. White and others, 2016; Knutz and others, 2019; Christ and others, 2020).

Evidence of alternation between deglacial conditions and subsequent glacial advances at NEEM is compatible with observations derived from the analysis of sub-ice sediment recovered closer to the northwestern GrIS margin, and at Camp Century, that evidenced two ice-free episodes since 3 Ma, the latest occurring within the last million year (Christ and others, 2021). These observations obtained from the NEEM core are in line with the hypothesis that the northwest margin of the GrIS was probably subject to more waning and waxing events than the central zone of Greenland during the Pleistocene, where 1 Ma old basal ice is preserved at GRIP (Willerslev and others, 2007; Yau and others, 2016a). However, future studies now need to constrain the absolute chronology of these oscillations evidenced in the NEEM basal ice record.

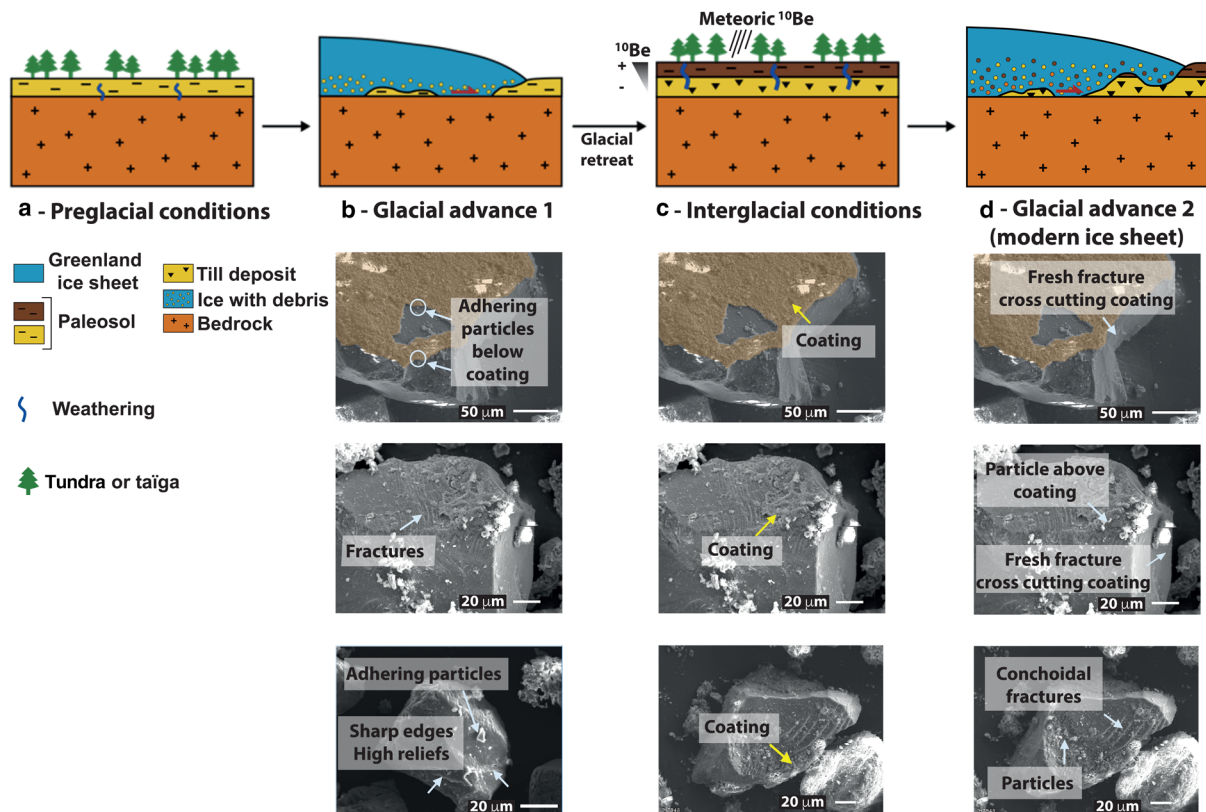


Figure 11. Diagrams illustrating the most probable scenarios of successive advances and retreats of the Greenland Ice Sheet at NEEM, mainly based on SEM imagery of the grains, meteoric ^{10}Be data and C/N, $\delta^{13}\text{C}$ measured in the basal debris. Upper cartoons are not to scale.

Supplementary material. The supplementary material for this article can be found at [10.24396/ORDAR-103](https://doi.org/10.24396/ORDAR-103).

Acknowledgements. This work is part of the international consortium for the study of basal-ice involving European (NBI Copenhagen, ULB Brussels, CRPG Nancy) and US (Vermont University, LDEO New York) research groups. P.-H. B. was funded by the program ‘Future Leader’ of Lorraine University of Excellence and by the ANR JC EroMed. We are grateful to two reviewers and to Editor M. Cassado for their constructive comments that improved the submitted version of the manuscript. The Post-Doc of M. P. was jointly financed by CNRS and the ANR JC EroMed program. Laurent Tissandier is kindly thanked for his assistance during the SEM analysis, as well as Florian Deman and David Verstraeten for their welcome in the VUB stable isotopes lab. P. C. thanks VUB Strategic Research and Research Foundation Flanders (FWO) Hercules foundation for instrument support. V. D. thanks the FRS-FNRS for support and the ERC StG ‘ISoSys’ for past funding. Sabrina Cauchies and Jeroen de Jong are thanked for support in the lab and Sm-Nd-Rb-Sr measurements.

Author contributions. P.-H. B., M. P., J.-L. T., F. P.: study design, ice core samples handling, data production, analysis, writing; M. P. notably realized the detailed SEM analysis, $^{10}\text{Be}_m$ and C/N data; D. D.-J., J. P. S.: study design, samples handling, data interpretation; W. C. M.: SEM imagery, data interpretation, writing; P. R. B., A. J. C., L. B. C.: $^{10}\text{Be}_m$ data, interpretation, writing; V. D.: Nd and Sr data, interpretation, writing; T. R. and P. C.: C/N data; ASTER Team: $^{10}\text{Be}/^9\text{Be}$ measurement.

References

- Arnold M and 8 others** (2010) The French accelerator mass spectrometry facility ASTER: improved performance and developments. *Nuclear Instruments and Methods in Physics Research Section B: Beam Interactions with Materials and Atoms* **268**(11), 1954–1959. doi: [10.1016/j.nimb.2010.02.107](https://doi.org/10.1016/j.nimb.2010.02.107)
- Barcilon V and MacAyeal D** (1993) Steady flow of a viscous ice stream across a no-slip free-slip transition at the bed. *Journal of Glaciology* **39**(131), 167–185. doi: [10.3189/S0022143000015811](https://doi.org/10.3189/S0022143000015811)
- Baumgartner S and 6 others** (1997) ^{10}Be and dust. *Nuclear Instruments and Methods in Physics Research Section B: Beam Interactions with Materials and Atoms* **123**(1–4), 296–301. doi: [10.1016/S0168-583X\(96\)00751-3](https://doi.org/10.1016/S0168-583X(96)00751-3)
- Bender ML, Burgess E, Alley RB, Barnett B and Clow GD** (2010) On the nature of the dirty ice at the bottom of the GISP2 ice core. *Earth and Planetary Science Letters* **299**(3), 466–473. doi: [10.1016/j.epsl.2010.09.033](https://doi.org/10.1016/j.epsl.2010.09.033)
- Bennike O and 5 others** (2010) Early Pleistocene sediments on Store Koldewey, northeast Greenland. *Boreas* **39**, 603–619.
- Bierman PR and 6 others** (2014) Preservation of a preglacial landscape under the center of the Greenland Ice Sheet. *Science* **344**(6182), 402–405. doi: [10.1126/science.1249047](https://doi.org/10.1126/science.1249047)
- Bierman PR, Shakun JD, Corbett LB, Zimmerman SR and Rood DH** (2016) A persistent and dynamic East Greenland Ice Sheet over the past 7.5 million years. *Nature* **540**(7632), 256–260. doi: [10.1038/nature20147](https://doi.org/10.1038/nature20147)
- Biscaye PE and 6 others** (1997) Asian provenance of glacial dust (stage 2) in the Greenland Ice Sheet Project 2 Ice Core, Summit, Greenland. *Journal of Geophysical Research: Oceans* **102**(C12), 26765–26781. doi: [10.1029/97JC01249](https://doi.org/10.1029/97JC01249)
- Bory AJ-M, Biscaye PE, Svensson A and Grousset FE** (2002) Seasonal variability in the origin of recent atmospheric mineral dust at NorthGRIP, Greenland. *Earth and Planetary Science Letters* **196**(3–4), 123–134. doi: [10.1016/S0012-821X\(01\)00609-4](https://doi.org/10.1016/S0012-821X(01)00609-4)
- Bory AJ-M, Biscaye PE and Grousset FE** (2003a) Two distinct seasonal Asian source regions for mineral dust deposited in Greenland (NorthGRIP). *Geophysical Research Letters* **30**(4), 2002GL016446. doi: [10.1029/2002GL016446](https://doi.org/10.1029/2002GL016446)
- Bory AJ-M, Biscaye PE, Piotrowski AM and Steffensen JP** (2003b) Regional variability of ice core dust composition and provenance in Greenland. *Geochemistry, Geophysics, Geosystems* **4**(12), 1–8. doi: [10.1029/2003GC000627](https://doi.org/10.1029/2003GC000627)
- Bourlès D, Raisbeck GM and Yiou F** (1989) ^{10}Be and ^9Be in marine sediments and their potential for dating. *Geochimica et Cosmochimica Acta* **53**(2), 443–452. doi: [10.1016/0016-7037\(89\)90395-5](https://doi.org/10.1016/0016-7037(89)90395-5)
- Braucher R and 6 others** (2015) Preparation of ASTER in-house $^{10}\text{Be}/^9\text{Be}$ standard solutions. *Nuclear Instruments and Methods in Physics Research Section B: Beam Interactions with Materials and Atoms* **361**, 335–340. doi: [10.1016/j.nimb.2015.06.012](https://doi.org/10.1016/j.nimb.2015.06.012)

- Cailleux A and Tricart J (1959) *Initiation à l'étude des sables et des galets*. Paris: Centre de la Documentation Universitaire.
- Callesen I, Raulund-Rasmussen K, Westman CJ and Tau-Strand L (2007) Nitrogen pools and C:N ratios in well-drained Nordic forest soils related to climate and soil texture. *Boreal Environment Research*, **12**, 681–692.
- Chauvel C and Blichert-Toft J (2001) A hafnium isotope and trace element perspective on melting of the depleted mantle. *Earth and Planetary Science Letters* **190**(3–4), 137–151. doi: [10.1016/S0012-821X\(01\)00379-X](https://doi.org/10.1016/S0012-821X(01)00379-X)
- Christ AJ and others (2020) The Northwestern Greenland Ice Sheet during the early Pleistocene was similar to today. *Geophysical Research Letters* **47**(1), e2019GL085176. doi: [10.1029/2019GL085176](https://doi.org/10.1029/2019GL085176)
- Christ AJ and 8 others (2021) A multimillion-year-old record of Greenland vegetation and glacial history preserved in sediment beneath 1.4 km of ice at Camp Century. *Proceedings of the National Academy of Sciences* **118**(13), e2021442118. doi: [10.1073/pnas.2021442118](https://doi.org/10.1073/pnas.2021442118)
- Christner BC, Montross GG and Priscu JC (2012) Dissolved gases in frozen basal water from the NGRIP borehole: implications for biogeochemical processes beneath the Greenland Ice Sheet. *Polar Biology* **35**(11), 1735–1741. doi: [10.1007/s00300-012-1198-z](https://doi.org/10.1007/s00300-012-1198-z)
- Collerson KD, McCulloch MT and Nutman AP (1989) Sr and Nd isotope systematics of polymetamorphic Archean gneisses from southern West Greenland and northern Labrador. *Canadian Journal of Earth Sciences* **26**(3), 446–466. doi: [10.1139/e89-039](https://doi.org/10.1139/e89-039)
- Corbett LB and 7 others (2021) Measuring multiple cosmogenic nuclides in glacial cobbles sheds light on Greenland Ice Sheet processes. *Earth and Planetary Science Letters* **554**, 116673. doi: [10.1016/j.epsl.2020.116673](https://doi.org/10.1016/j.epsl.2020.116673)
- Dahl-Jensen D and 132 others (2013) Eemian interglacial reconstructed from a Greenland folded ice core. *Nature* **493**(7433), 489–494. doi: [10.1038/nature11789](https://doi.org/10.1038/nature11789)
- Dawes PR (2009) The bedrock geology under the Inland Ice: the next major challenge for Greenland mapping. *GEUS Bulletin* **17**, 57–60. doi: [10.34194/geusb.v17.5014](https://doi.org/10.34194/geusb.v17.5014)
- de Angelis M, Tison J-L, Morel-Fourcade M-C and Susini J (2013) Micro-investigation of EPICA Dome C bottom ice: evidence of long term in situ processes involving acid–salt interactions, mineral dust, and organic matter. *Quaternary Science Reviews* **78**, 248–265. doi: [10.1016/j.quascirev.2013.08.012](https://doi.org/10.1016/j.quascirev.2013.08.012)
- de Vernal A and Hillaire-Marcel C (2008) Natural variability of Greenland climate, vegetation, and ice volume during the past million years. *Science* **320**(5883), 1622–1625. doi: [10.1126/science.1153929](https://doi.org/10.1126/science.1153929)
- de Vernal A and Mudie P (1989) Late Pliocene to Holocene palynostratigraphy at ODP site 645, Baffin Bay. Proc., Scientific Results, ODP, Leg 105, Baffin Bay and Labrador Sea 105, 387–399. doi: [10.2973/odp.proc.sr.105.133.1989](https://doi.org/10.2973/odp.proc.sr.105.133.1989)
- Diaz MA and 7 others (2021) Relationship between meteoric ^{10}Be and NO_3^- concentrations in soils along Shackleton Glacier, Antarctica. *Earth Surface Dynamics* **9**(5), 1363–1380. doi: [10.5194/esurf-9-1363-2021](https://doi.org/10.5194/esurf-9-1363-2021)
- Drucker DG, Hobson KA, Ouellet J-P and Courtois R (2010) Influence of forage preferences and habitat use on ^{13}C and ^{15}N abundance in wild caribou (*Rangifer tarandus caribou*) and moose (*Alces alces*) from Canada. *Isotopes in Environmental and Health Studies* **46**(1), 107–121. doi: [10.1080/10256010903388410](https://doi.org/10.1080/10256010903388410)
- Dutton A and 8 others (2015) Sea-level rise due to polar ice-sheet mass loss during past warm periods. *Science* **349**(6244), aaa4019. doi: [10.1126/science.aaa4019](https://doi.org/10.1126/science.aaa4019)
- Ernakovich JG, Wallenstein MD and Calderón FJ (2015) Chemical indicators of cryoturbation and microbial processing throughout an Alaskan permafrost soil depth profile. *Soil Science Society of America Journal* **79**(3), 783–793. doi: [10.2136/sssaj2014.10.0420](https://doi.org/10.2136/sssaj2014.10.0420)
- Folk RL (1975) Glacial deposits identified by chattermark trails in detrital garnets. *Geology* **3**(8), 473–475.
- Fountain J, Usselman TM, Wooden J and Langway CC (1981) Evidence of the bedrock beneath the Greenland Ice Sheet near Camp Century, Greenland. *Journal of Glaciology* **27**(95), 193–197. doi: [10.3189/S0022143000011370](https://doi.org/10.3189/S0022143000011370)
- Funder S and 5 others (2001). Late Pliocene Greenland—the Kap København formation in North Greenland. *Bulletin of the Geological Society of Denmark* **48**, 117–134.
- Funder S, Abrahamsen N, Bennike O and Feyling-Hanssen RW (1985) Forested Arctic: evidence from North Greenland. *Geology* **13**(8), 542–546. doi: [10.1130/0091-7613\(1985\)13<542:FAEFNG>2.0.CO;2](https://doi.org/10.1130/0091-7613(1985)13<542:FAEFNG>2.0.CO;2)
- Goossens T and 5 others (2016) A comprehensive interpretation of the NEEM basal ice build-up using a multi-parametric approach. *The Cryosphere* **10**(2), 553–567. doi: [10.5194/tc-10-553-2016](https://doi.org/10.5194/tc-10-553-2016)
- Graly JA, Bierman PR, Reusser LJ and Pavich MJ (2010) Meteoric ^{10}Be in soil profiles – a global meta-analysis. *Geochimica et Cosmochimica Acta* **74**(23), 6814–6829. doi: [10.1016/j.gca.2010.08.036](https://doi.org/10.1016/j.gca.2010.08.036)
- Graly JA, Corbett LB, Bierman PR, Lini A and Neumann TA (2018) Meteoric ^{10}Be as a tracer of subglacial processes and interglacial surface exposure in Greenland. *Quaternary Science Reviews* **191**, 118–131. doi: [10.1016/j.quascirev.2018.05.009](https://doi.org/10.1016/j.quascirev.2018.05.009)
- Hart KM and 7 others (2011) A bacterial enrichment study and overview of the extractable lipids from paleosols in the dry valleys, Antarctica: implications for future Mars reconnaissance. *Astrobiology* **11**(4), 303–321. doi: [10.1089/ast.2010.0583](https://doi.org/10.1089/ast.2010.0583)
- Harwood DM (1986) Do diatoms beneath the Greenland Ice Sheet indicate interglacials warmer than present? *Arctic* **39**(4), 304–308.
- Hugelius G, Kuhry P, Tarnocai C and Virtanen T (2010) Soil organic carbon pools in a periglacial landscape: a case study from the central Canadian Arctic. *Permafrost and Periglacial Processes* **21**(1), 16–29. doi: [10.1002/ppp.677](https://doi.org/10.1002/ppp.677)
- Jungers MC and 5 others (2009) Tracing hillslope sediment production and transport with in situ and meteoric ^{10}Be . *Journal of Geophysical Research: Earth Surface* **114**(F4), F04020. doi: [10.1029/2008JF001086](https://doi.org/10.1029/2008JF001086)
- Kirkland CL, Pease V, Whitehouse MJ and Ineson JR (2009) Provenance record from Mesoproterozoic-Cambrian sediments of Peary Land, North Greenland: implications for the ice-covered Greenland Shield and Laurentian palaeogeography. *Precambrian Research* **170**(1), 43–60. doi: [10.1016/j.precamres.2008.11.006](https://doi.org/10.1016/j.precamres.2008.11.006)
- Knight PG (1997) The basal ice layer of glaciers and ice sheets. *Quaternary Science Reviews* **16**(9), 975–993. doi: [10.1016/S0277-3791\(97\)00033-4](https://doi.org/10.1016/S0277-3791(97)00033-4)
- Knutz PC and 6 others (2019) Eleven phases of Greenland Ice Sheet shelf-edge advance over the past 2.7 million years. *Nature Geoscience* **12**(5), 361–368. doi: [10.1038/s41561-019-0340-8](https://doi.org/10.1038/s41561-019-0340-8)
- Larsen HC and 5 others (1994) Seven million years of glaciation in Greenland. *Science* **264**(5161), 952–955. doi: [10.1126/science.264.5161.952](https://doi.org/10.1126/science.264.5161.952)
- Larsen NK and 9 others (2021) Cosmogenic nuclide inheritance in Little Ice Age moraines – a case study from Greenland. *Quaternary Geochronology* **65**, 101200. doi: [10.1016/j.quageo.2021.101200](https://doi.org/10.1016/j.quageo.2021.101200)
- Lewis AR and 12 others (2008) Mid-Miocene cooling and the extinction of tundra in continental Antarctica. *Proceedings of the National Academy of Sciences* **105**(31), 10676–10680. doi: [10.1073/pnas.0802501105](https://doi.org/10.1073/pnas.0802501105)
- MacGregor JA and 11 others (2015) Radar attenuation and temperature within the Greenland Ice Sheet. *Journal of Geophysical Research: Earth Surface* **120**(6), 983–1008. doi: [10.1002/2014JF003418](https://doi.org/10.1002/2014JF003418)
- Mahaney W (1995) Glacial crushing, weathering and diagenetic histories of quartz grains inferred from scanning electron microscopy. *Glacial Environments – Processes, Sediments and Landforms*, **24**, 487–506.
- Mahaney WC (2002) *Atlas of Sand Grain Surface Textures and Applications*. Oxford: Oxford University Press, 237 p.
- Mahaney WC (2015) Pedological iron/Al extracts, clast analysis, and Coleoptera from Antarctic paleosol 831: evidence of a Middle Miocene or earlier climatic optimum. *The Journal of Geology* **123**(2), 113–132. doi: [10.1086/680339](https://doi.org/10.1086/680339)
- Mahaney WC and Schwartz S (2021) Clast rind-paleosol record of the Antarctic early Alpine glaciation. *Polar Science* **28**, 100648. doi: [10.1016/j.polar.2021.100648](https://doi.org/10.1016/j.polar.2021.100648)
- Mahaney W, Stewart A and Kalm V (2001) Quantification of SEM microtextures in sedimentary environmental discrimination. *Boreas* **30**, 165–171. doi: [10.1080/030094801750203170](https://doi.org/10.1080/030094801750203170)
- Mahaney WC and 11 others (2013) Weathering rinds as mirror images of palaeosols: examples from the Western Alps with correlation to Antarctica and Mars. *Journal of the Geological Society* **170**(5), 833–847. doi: [10.1144/jgs2012-150](https://doi.org/10.1144/jgs2012-150)
- Marty C, Houle D, Gagnon C and Courchesne F (2017) The relationships of soil total nitrogen concentrations, pools and C:N ratios with climate, vegetation types and nitrate deposition in temperate and boreal forests of eastern Canada. *CATENA* **152**, 163–172. doi: [10.1016/j.catena.2017.01.014](https://doi.org/10.1016/j.catena.2017.01.014)
- Meyers PA (1994) Preservation of elemental and isotopic source identification of sedimentary organic matter. *Chemical Geology* **114**(3–4), 289–302. doi: [10.1016/0009-2541\(94\)90059-0](https://doi.org/10.1016/0009-2541(94)90059-0)
- Nagatsuka N and 6 others (2016) Variations in Sr and Nd isotopic ratios of mineral particles in cryoconite in Western Greenland. *Frontiers in Earth Science* **4**. doi: [10.3389/feart.2016.00093](https://doi.org/10.3389/feart.2016.00093)
- Nelson AH, Bierman PR, Shakun JD and Rood DH (2014) Using in situ cosmogenic ^{10}Be to identify the source of sediment leaving Greenland. *Earth Surface Processes and Landforms* **39**(8), 1087–1100. doi: [10.1002/esp.3565](https://doi.org/10.1002/esp.3565)

- Nishiizumi K and 5 others** (2007) Absolute calibration of ^{10}Be AMS standards. *Nuclear Instruments and Methods in Physics Research Section B: Beam Interactions with Materials and Atoms* **258**(2), 403–413. doi: [10.1016/j.nimb.2007.01.297](https://doi.org/10.1016/j.nimb.2007.01.297)
- Oelbermann M and Voroney RP** (2007) Carbon and nitrogen in a temperate agroforestry system: using stable isotopes as a tool to understand soil dynamics. *Ecological Engineering* **29**(4), 342–349. doi: [10.1016/j.ecoleng.2006.09.014](https://doi.org/10.1016/j.ecoleng.2006.09.014)
- Pavich MJ, Brown L, Klein J and Middleton R** (1984) ^{10}Be accumulation in a soil chronosequence. *Earth and Planetary Science Letters* **68**(2), 198–204. doi: [10.1016/0012-821X\(84\)90151-1](https://doi.org/10.1016/0012-821X(84)90151-1)
- Puchol N and 6 others** (2017) Limited impact of quaternary glaciations on denudation rates in Central Asia. *GSA Bulletin* **129**(3–4), 479–499. doi: [10.1130/B31475.1](https://doi.org/10.1130/B31475.1)
- Schaefer JM and 8 others** (2016) Greenland was nearly ice-free for extended periods during the Pleistocene. *Nature* **540**(7632), 252–255. doi: [10.1038/nature20146](https://doi.org/10.1038/nature20146)
- Simon Q and 5 others** (2016) Authigenic $^{10}\text{Be}/^9\text{Be}$ ratios and ^{10}Be -fluxes (^{230}Th s-normalized) in central Baffin Bay sediments during the last glacial cycle: paleoenvironmental implications. *Quaternary Science Reviews* **140**, 142–162. doi: [10.1016/j.quascirev.2016.03.027](https://doi.org/10.1016/j.quascirev.2016.03.027)
- Simonsen MF and 15 others** (2019) East Greenland ice core dust record reveals timing of Greenland ice sheet advance and retreat. *Nature Communications* **10**(1), 4494. doi: [10.1038/s41467-019-12546-2](https://doi.org/10.1038/s41467-019-12546-2)
- Smalley IJ** (1966) The properties of glacial loess and formation of loess deposits. *Journal of Sedimentary Research* **36**, 669–676.
- Souchez R and 8 others** (1994) Stable isotopes in the basal silty ice preserved in the Greenland Ice Sheet at summit; environmental implications. *Geophysical Research Letters* **21**(8), 693–696. doi: [10.1029/94GL00641](https://doi.org/10.1029/94GL00641)
- Souchez R and 5 others** (2006) Gas isotopes in ice reveal a vegetated central Greenland during ice sheet invasion. *Geophysical Research Letters* **33**(24), L24503. doi: [10.1029/2006GL028424](https://doi.org/10.1029/2006GL028424)
- Souchez R, Janssens L, Lemmens M and Stauffer B** (1995) Very low oxygen concentration in basal ice from Summit, central Greenland. *Geophysical Research Letters* **22**(15), 2001–2004. doi: [10.1029/95GL01995](https://doi.org/10.1029/95GL01995)
- Souchez R, Vandenschrick G, Lorrain R and Tison J-L** (2000) Basal ice formation and deformation in central Greenland: a review of existing and new ice core data. *Geological Society, London, Special Publications* **176**(1), 13–22. doi: [10.1144/GSL.SP.2000.176.01.02](https://doi.org/10.1144/GSL.SP.2000.176.01.02)
- Stone J** (1998) A rapid fusion method for separation of beryllium-10 from soils and silicates. *Geochimica et Cosmochimica Acta* **62**(3), 555–561. doi: [10.1016/S0016-7037\(97\)00340-2](https://doi.org/10.1016/S0016-7037(97)00340-2)
- Sturevik-Storm A and 7 others** (2015) ^{10}Be climate fingerprints during the Eemian in the NEEM ice core, Greenland. *Scientific Reports* **4**(1), 6408. doi: [10.1038/srep06408](https://doi.org/10.1038/srep06408)
- Svensson A, Biscaye PE and Grousset FE** (2000) Characterization of late glacial continental dust in the Greenland Ice Core Project ice core. *Journal of Geophysical Research: Atmospheres* **105**(D4), 4637–4656. doi: [10.1029/1999JD901093](https://doi.org/10.1029/1999JD901093)
- Tison J-L and 5 others** (1998) Is a periglacial biota responsible for enhanced dielectric response in basal ice from the Greenland Ice Core Project ice core? *Journal of Geophysical Research: Atmospheres* **103**(D15), 18885–18894. doi: [10.1029/98JD01107](https://doi.org/10.1029/98JD01107)
- Tison J-L and 8 others** (2019) A census of basal ice samples from deep ice cores at NBI. Available at <https://hal-cnrs.archives-ouvertes.fr/hal-03420093>
- Tison J-L, Petit J-R, Barnola J-M and Mahaney WC** (1993) Debris entrainment at the ice-bedrock interface in sub-freezing temperature conditions (Terre Adélie, Antarctica). *Journal of Glaciology* **39**(132), 303–315. doi: [10.3189/S0022143000015963](https://doi.org/10.3189/S0022143000015963)
- Tison J-L, Thorsteinsson T, Lorrain RD and Kipfstuhl J** (1994) Origin and development of textures and fabrics in basal ice at Summit, Central Greenland. *Earth and Planetary Science Letters* **125**(1–4), 421–437. doi: [10.1016/0012-821X\(94\)90230-5](https://doi.org/10.1016/0012-821X(94)90230-5)
- Tripati A and Darby D** (2018) Evidence for ephemeral middle Eocene to early Oligocene Greenland glacial ice and pan-Arctic sea ice. *Nature Communications* **9**(1), 1038. doi: [10.1038/s41467-018-03180-5](https://doi.org/10.1038/s41467-018-03180-5)
- Urrea A and 9 others** (2019) Weathering dynamics under contrasting Greenland ice sheet catchments. *Frontiers in Earth Science* **7**. doi: [10.3389/feart.2019.00299](https://doi.org/10.3389/feart.2019.00299)
- Verbeke V, Lorrain R, Johnsen SJ and Tison J-L** (2002) A multiple-step deformation history of basal ice from the Dye 3 (Greenland) core: new insights from the CO_2 and CH_4 content. *Annals of Glaciology* **35**, 231–236. doi: [10.3189/172756402781817248](https://doi.org/10.3189/172756402781817248)
- Wasserburg GJ, Jacobsen SB, De Paolo DJ, McCulloch MT and Wen T** (1981) Precise determination of Sm/Nd ratios, Sm and Nd isotopic abundances in standard solutions. *Geochimica et Cosmochimica Acta* **45**, 2311–2323.
- Weis D, Demaiffe D, Souchez R, Gow AJ and Meese DA** (1997) Ice sheet development in central Greenland: implications from the Nd, Sr and pH isotopic compositions of basal material. *Earth and Planetary Science Letters* **150**(1–2), 161–169. doi: [10.1016/S0012-821X\(97\)00073-3](https://doi.org/10.1016/S0012-821X(97)00073-3)
- Weis D and 12 others** (2006) High-precision isotopic characterization of USGS reference materials by TIMS and MC-ICP-MS: Isotopic study of USGS reference materials. *Geochemistry, Geophysics, Geosystems* **7**(8), Q08006. doi: [10.1029/2006GC001283](https://doi.org/10.1029/2006GC001283)
- Westerhold T and 23 others** (2020) An astronomically dated record of Earth's climate and its predictability over the last 66 million years. *Science* **369**(6509), 1383–1387. doi: [10.1126/science.aba6853](https://doi.org/10.1126/science.aba6853)
- Whalley WB and Langway CC Jr.** (1980) A scanning electron microscope examination of subglacial quartz grains from Camp Century core, Greenland – a preliminary study. *Journal of Glaciology* **25**(91), 125–132.
- White LF and 8 others** (2016) Tracking the provenance of Greenland-sourced, Holocene aged, individual sand-sized ice-rafted debris using the Pb-isotope compositions of feldspars and $^{40}\text{Ar}/^{39}\text{Ar}$ ages of hornblendes. *Earth and Planetary Science Letters* **433**, 192–203. doi: [10.1016/j.epsl.2015.10.054](https://doi.org/10.1016/j.epsl.2015.10.054)
- Willenbring JK and von Blanckenburg F** (2010) Meteoric cosmogenic Beryllium-10 adsorbed to river sediment and soil: applications for Earth-surface dynamics. *Earth-Science Reviews* **98**(1), 105–122. doi: [10.1016/j.earscirev.2009.10.008](https://doi.org/10.1016/j.earscirev.2009.10.008)
- Willerslev E and 29 others** (2007) Ancient biomolecules from deep ice cores reveal a forested southern Greenland. *Science* **317**(5834), 111–114. doi: [10.1126/science.1141758](https://doi.org/10.1126/science.1141758)
- Wittmann H and 9 others** (2015) A test of the cosmogenic ^{10}Be (meteoric)/ ^9Be proxy for simultaneously determining basin-wide erosion rates, denudation rates, and the degree of weathering in the Amazon basin: erosion from meteoric $^{10}\text{Be}/^9\text{Be}$ in Amazon. *Journal of Geophysical Research: Earth Surface* **120**(12), 2498–2528. doi: [10.1002/2015JF003581](https://doi.org/10.1002/2015JF003581)
- Woronko B** (2016) Frost weathering versus glacial grinding in the micromorphology of quartz sand grains: processes and geological implications. *Sedimentary Geology* **335**, 103–119. doi: [10.1016/j.sedgeo.2016.01.021](https://doi.org/10.1016/j.sedgeo.2016.01.021)
- Xu X, Thornton PE and Post WM** (2013) A global analysis of soil microbial biomass carbon, nitrogen and phosphorus in terrestrial ecosystems: global soil microbial biomass C, N and P. *Global Ecology and Biogeography* **22**(6), 737–749. doi: [10.1111/geb.12029](https://doi.org/10.1111/geb.12029)
- Yau AM, Bender ML, Blunier T and Jouzel J** (2016a) Setting a chronology for the basal ice at Dye-3 and GRIP: implications for the long-term stability of the Greenland Ice Sheet. *Earth and Planetary Science Letters* **451**, 1–9. doi: [10.1016/j.epsl.2016.06.053](https://doi.org/10.1016/j.epsl.2016.06.053)
- Yau AM, Bender ML, Robinson A and Brook EJ** (2016b) Reconstructing the last interglacial at Summit, Greenland: insights from GISP2. *Proceedings of the National Academy of Sciences* **113**(35), 9710–9715. doi: [10.1073/pnas.1524766113](https://doi.org/10.1073/pnas.1524766113)